SPONTANEOUS FOUR-WAVE MIXING IN STANDARD BIREFRINGENT FIBER

by

Jamy B. Moreno

A thesis submitted to the Faculty of the University of Delaware in partial fulfillment of the requirements for the degree of Master of Science in Physics and Astronomy

Spring 2012

© 2012 Jamy B. Moreno
All Rights Reserved

SPONTANEOUS FOUR-WAVE MIXING

IN STANDARD BIREFRINGENT FIBER

by

Jamy B. Moreno

Approved: _____

Virginia Lorenz, Ph.D.
Professor in charge of thesis on behalf of the Advisory Committee

Approved: _____

George Hadjipanayas, Ph.D.
Chair of the Department of Physics and Astronomy

Approved: _____

George H. Watson, Ph.D.
Dean of the College of Arts and Sciences

Approved: _____

Charles G. Riordan, Ph.D.
Vice Provost for Graduate and Professional Education

ACKNOWLEDGMENTS

First and foremost I would like to thank my advisor, Professor Virginia Lorenz, who has guided and supported me throughout my whole graduate career. She has been a source of inspiration and has always believed in me, and for that I thank her.

I would like to give my most sincerest thanks to Offir Cohen who has worked closely with me from when I started up until I finished. Thank you for your patience and your knowledge. I have learned so much from you.

I would like to also extend my thanks to my committee members Professor Matthew DeCamp and Professor Jamie Holder for their guidance.

I would like thank the members of the Ultrafast group Seth Meiselman, Bin Fang, and Halise Celik. Not only did they provide useful discussions and insight, but they also made for a wonderful and fun group to work with.

To all the friends I have made here at the University of Delaware, thank you for making my graduate experience a wonderful one. Particular thanks goes to Kevin Haughey. Thanks for everything. I would also like to give my thanks to my officemates, my best friends here, the "chicas": Katie Mulrey, Inci Ruzybayev, and Han Zou. The past few years would definitely not have been nearly as fun without you.

Lastly, I would like to thank my family. Thank you for being so understanding and supportive through everything. I could not have done it without you.

TABLE OF CONTENTS

LIST OF FIGURES . . . . . **vi**
ABSTRACT . . . . . **vii**

Chapter

1 INTRODUCTION **1**

1.1 Linear-Optics Quantum-Computation 1
1.2 Hong-Ou-Mandel (HOM) Interference 2
1.3 Single Photon Generators 3

1.3.1 Single-Emitter Photon Sources 4
1.3.2 Heralded Photons 4

1.4 Standard Fibers 6
1.5 Phasematching and Energy Conservation in SFWM 7
1.6 Outline 8

2 SPONTANEOUS FOUR-WAVE MIXING USING DEGENERATE PUMP PHOTONS: EXPERIMENTAL IMPLEMENTATION . . **9**

2.1 Birefringent Standard Fibers 9
2.2 Phasematching for Degenerate Pump Photons 10
2.3 Experimental Setup 11

2.3.1 Second-Order Coherence Function 14
2.3.2 Heralding Efficiency 15

3 SPONTANEOUS FOUR-WAVE MIXING USING NON-DEGENERATE PUMP PHOTONS: A THEORETICAL STUDY **17**

3.1 Phasematching for Non-Degenerate Pump Photons 17

3.2 Joint Spectral Amplitude 19
3.3 Interaction in the Fiber 22

3.3.1 Regime 1: negligible temporal walk-off between the two pump beams ($|\sigma\tau_p| << 1$) 24
3.3.2 Regime 2: $|\sigma\tau_p| >> 1$ 24

3.4 Purity and Factorability 26
3.5 Numerical Methods 28

4 SUMMARY 31

4.1 Conclusion 31

BIBLIOGRAPHY 33

Appendix

A JOINT SPECTRAL AMPLITUDE CALCULATION 35

A.1 Regime 1 calculation 41
A.2 Regime 2 calculation 42

LIST OF FIGURES

1.1 Hong-Ou-Mandel Interference 3

1.2 Heralded Photons 5

1.3 Step-Index Model for Standard Fibers 7

2.1 Phasematching plot for degenerate pump photons 12

2.2 Experimental setup of SFWM process using degenerate pump photons 13

2.3 Normalized spectra using Fibercore 800G 14

3.1 Phasematching plot for nondegenerate pump photons 18

3.2 Energy conservation, phasematching, and joint spectrum for $\Delta\lambda$ =45 nm 23

3.3 Calculated Joint spectral amplitude in the regime when $\sigma\tau_p, \sigma\tau << 1$ 25

3.4 Joint spectral amplitude in the regime when $|\sigma\tau_p|, |\sigma\tau| >> 1$ . . . 26

3.5 Joint spectral probability for detunings $\Delta\lambda$ = 50 nm, 150 nm, and 240 nm with central wavelength $\lambda_p = 700$ nm 29

3.6 Purity and $\min\{|f_{p1} - f_s|, |f_{p1} - f_i|\}$ as a function of detuning, $\Delta\lambda$, in the regime where $|\sigma\tau_p| >> 1$. $\tau = -\frac{1}{2}\tau_p$ 30

ABSTRACT

This thesis presents an experimental implementation and a theoretical investigation of a source of photon-pairs. The source is based on the nonlinear optical interaction of two strong pump pulses in a birefringent single-mode optical fiber. The interaction is mediated by the $\chi^{(3)}$ susceptibility of the fiber medium and results in the spontaneous creation of two photons, referred to as the signal and idler. Because the signal and idler photons are produced simultaneously, one of the photons can be used to *herald* the other. The creation of photons in such a fiber is motivated by the fact that their mode is matched for coupling into quantum information networks that are composed of similar fibers. Indeed, such a photon-pair source has already been shown to be capable of producing photon-pairs that are suitable for quantum computing and quantum communication applications.

In this thesis we experimentally confirm that photon pairs can be generated through this type of fiber, using degenerate pump pulses. We then investigate theoretically the spectral correlations introduced between the photons when they are created by two pump pulses with different wavelengths. We find that the group velocity difference between the two pumps can be utilized to switch the nonlinear optical interaction on and off gradually, and showed that this feature can be employed for the creation of 100% uncorrelated photon pairs, which is a necessary condition for the heralding of pure single photons.

Chapter 1

INTRODUCTION

1.1 Linear-Optics Quantum-Computation

With the advancement of information technology, systems are becoming smaller, thus requiring a quantum mechanical description. In 1985, David Deutsch laid the foundations for the field of quantum computation [1], by proposing logic gates operating on quantum systems. Quantum computation exploits the superposition principle and non-classical correlations of quantum mechanics.

While a classical computer uses bits that take values of either zero or one to store information, a quantum computer utilizes qubits. A qubit can represent a zero, a one, or any superposition of these states. In general, a quantum computer that has n qubits can be in a superposition of up to 2^n different states simultaneously, compared to a classical computer that can only be in one of the 2^n states at a time. Because of this fact, it is believed that quantum computers are able to solve problems much faster than classical computers.

Shor's algorithm [2] is a quantum algorithm that finds the prime factors of an integer N. When implemented, this algorithm takes a time that goes as a polynomial of N, a much faster time than that of a classical computer whose computation time is $\sim \exp(N^{\frac{1}{3}})$. Because of this, Shor's algorithm, when employed on a quantum computer with a sufficient number of qubits, can be used to break public-key cryptography schemes including the commonly used RSA scheme, illustrating one of the many applications of quantum computation.

As stated above, a qubit is the quantum counterpart to a classical bit. It is the basic unit of quantum computation. One good candidate for implementing a qubit is

the photon since it rarely interacts with its environment and is ideal for information transfer over large distances [3]. It was believed that to obtain scalable quantum information processing, nonlinear couplings between optical modes was necessary, until 2001 when Knill, Laflamme, and Milburn (KLM) proposed a scheme for quantum computation using linear optics [4].

In order to implement the so-called linear optics quantum computation (LOQC) scheme, three nontrivial resources have to be available: quantum memories, photon counting detectors, and single photon generators. Research has been conducted and produced viable methods for the first resource, namely, state storage and retrieval [5]. Photon counting detectors have also been studied and research in this area has provided methods for photon-number resolving detection [6].

The third nontrivial resource, a single photon generator, needs to be a source that produces the same photon each and every time in order to use it for the LOQC scheme. Identical and indistinguishable photons will undergo Hong-Ou-Mandel (HOM) interference, which is described in the next section. This thesis presents a method to realize such a source.

1.2 Hong-Ou-Mandel (HOM) Interference

The Hong-Ou-Mandel (HOM) interference is a two-photon interference that takes place when two identical and indistinguishable photons interfere on a 50% beam splitter, as shown in figure 1.1.

Assume we have two photons that are identical in every degree of freedom such that they have the same polarization and spectral-temporal shape, and are also in a pure wave-packet. In a lossless beamsplitter, a photon that is reflected picks up a $\pi/2$ phase relative to the transmitted photon [8]. Therefore, the situation when the two identical photons are reflected destructively interferes with the situation when both photons are transmitted, as shown in the top picture in figure 1.1. Thus, the two photons bunch together in the same arm, yielding a superposition of both photons being in either arm, as depicted in the lower picture of figure 1.1.

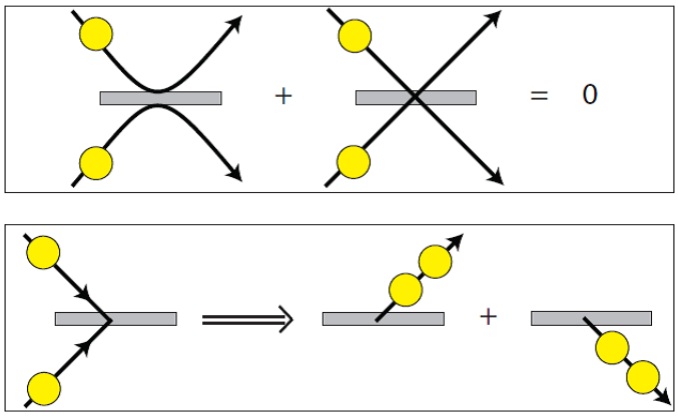

Figure 1.1: Two identical photons interfering on a 50% lossless beamsplitter. The case when both photons are reflected destructively interferes with the situation when they are both transmitted (top). The resulting two-photon state is then a superposition of both photons bunching together and leaving the beamsplitter at the same arm (bottom).

For photon sources to be applied to an LOQC scheme, they have to produce photons that interfere in such a fashion, i.e. that are pure and identical.

1.3 Single Photon Generators

An ideal single photon source emits a single photon in each triggering event. This is different than a "classical" source such as an attenuated laser, where the number of photons in each pulse follows a Poissonian distribution, and hence does not contain necessarily one and only one photon.

To date, there are two main techniques to generate single photons. The first technique uses a single emitting system that produces photons via spontaneous emission. The second technique randomly produces photons, although always in pairs. The pair is created simultaneously; therefore, the detection of one photon implies the presence of the other. Such a photon is considered a *heralded* photon.

1.3.1 Single-Emitter Photon Sources

An example of a single-emitter photon source that has already been implemented is an atom trapped in a cavity via a dipole trap. A single photon can be generated on-demand by applying a laser pulse to the trapped atom. The cavity is comprised of two highly reflective mirrors and its purpose is to ensure that all photons generated are sent in the same spatial mode. This method produces single photons whose energy varies very little [9]. However, the experimental setup is highly complicated and requires several laser beams and stabilized cavities.

Instead of using a cavity, a molecule may be used and trapped inside a matrix to form an on-demand single photon source. However, since molecules have many vibrational levels available, the trapped molecule must be kept under cryogenic conditions [10, 11] so as to suppress these vibrational levels. This again poses an inconvenience because of its complexity.

Quantum dots may also serve as a viable single photon emitter. Similar to trapped molecules, the quantum dots must be kept under cryogenic conditions. The produced photons vary in energy and are distinguishable, making them unusable for the LOQC scheme.

The examples of single emitters stated above are indeed realizable on-demand single-emitter photon sources, however, they suffer from either the complex nature of the experimental setup, and/or the distinguishability of the generated photons.

1.3.2 Heralded Photons

The technique of heralded photon generation described in this section randomly produces photons, but always in pairs. Therefore, the presence of one *heralds* the other. The experimental implementation of heralded photons is simple compared to the single-photon emitters described in the previous section and therefore have been widely used. There are two common methods to produce heralded photons; the first is called spontaneous parametric down conversion (SPDC), the other is called spontaneous four-wave mixing (SFWM).

SPDC is a three-wave mixing process in which a single pump photon produces a photon-pair via a nonlinear process that is mediated by a $\chi^{(2)}$ nonlinear susceptibility. Materials whose leading non-linear susceptibility term is the $\chi^{(2)}$ term include bulk crystals such as beta-barium borate (BBO). An external electromagnetic field, the pump, is annihilated by the medium, then produces two daughter photons [12]. Both daughter photons are created simultaneously, and therefore, one *heralds* the other.

This technique of heralding has been applied to another process, namely, spontaneous four-wave mixing (SFWM), which is the process we focus on in this thesis. In this case, the process is mediated by a $\chi^{(3)}$ nonlinear susceptibility, wherein two pump photons (as opposed to only one in the case of SPDC) that are not necessarily degenerate are annihilated by the medium, and then produce two different photons, called the signal and idler. In amorphous materials like glass, the leading nonlinear susceptibility term is the $\chi^{(3)}$ term.

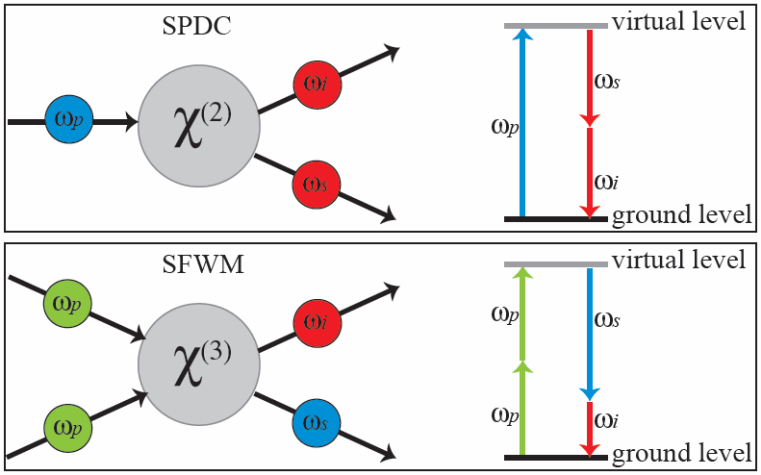

Figure 1.2: Schematic and energy-level diagram for SPDC (top). For this process, a single pump photon is annihilated in a medium with a $\chi^{(2)}$ susceptibility and produces two daughter photons. The bottom illustrates a SFWM (bottom) interaction and corresponding energy-level diagram. A SFWM process is mediated by a $\chi^{(3)}$ susceptibility. Two (not necessarily) degenerate pump photons are annihilated in the medium and then produce a signal and idler photon.

Figure 1.2 illustrate a schematic of an SPDC and SFWM process. In both cases,

energy must be conserved (see level diagram). For the case of SPDC, the frequency of the pump photon must be equal to the sum of frequencies of the daughter photons. In SFWM, the frequency of two pump photons (not necessarily degenerate) must sum up to the frequencies of the generated photon pair.

It should be noted that a SFWM process has the flexibility to use any two pump photons and generate signal and idler photons (that satisfy both energy and momentum conservation), unlike the SPDC process that is limited to just a single pump. Because of this, we have chosen to further investigate SFWM, specifically in standard optical fibers.

1.4 Standard Fibers

An optical fiber is made of thin glass and functions as a waveguide that confines light through total internal reflection. As a result, light travels though the fiber with low loss. Due to their spatial modes, optical fibers are good sources for quantum computation and communication networks that utilize fibers or waveguides. The step-index model can be used to describe a standard fiber in the following way: Fibers consists of two concentric cylinders making the core and cladding, as seen in figure 1.3. The core of radius a, is made up of a dispersive material with an index of refraction $n_1(\omega)$ that is dependent on frequency, ω. The cladding is made of a material with a refractive index, also dependent on frequency, lower than that of the core, $n_2(\omega) < n_1(\omega)$.

Most of the fibers' core and cladding are made of silica. The core is usually doped with germanium dioxide and/or aluminum dioxide to increase the core's refractive index, while the cladding is generally doped with flourine, boron trioxide or rare earth metals to decrease the cladding's refractive index [3].

The spatial modes traveling through the fiber are given by the solutions to Maxwell's equations in the core and cladding such that energy propagates only in the z direction and not outside of the fiber. Each mode experiences an effective index of refraction, n_{eff}, such that $n_2 < n_{eff} < n_1$.

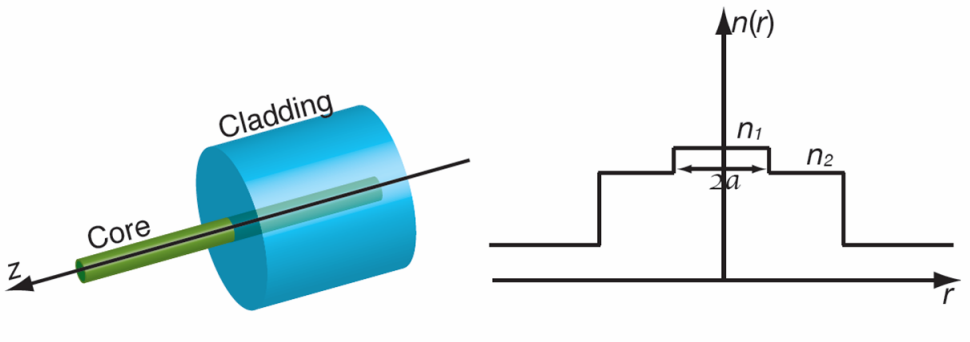

Figure 1.3: The step-index model for a standard fiber. The core with radius a and index of refraction n_1 is encased in a cladding with refractive index n_2 such that $n_1 > n_2$.

In general, several spatial modes can exist, but not in the case when a single mode fiber is used. Single-mode fibers, whose core is so narrow (less than 10 μm), support only one spatial mode. We assume the use of single mode fibers in this thesis.

1.5 Phasematching and Energy Conservation in SFWM

As stated previously, a SFWM process must satisfy both momentum and energy conservation. The momentum conservation constraint is called the phase-matching condition. The wave-vectors associated with each mode, k_μ, where $\mu = p_1, p_2, s, i$, for pump 1, pump 2, signal, and idler respectively, satisfy the phase-matching condition:

$$\Delta k = k_{p1}(\omega_{p1}) + k_{p2}(\omega_{p2}) - k_s(\omega_s) - k_i(\omega_i) = 0 \tag{1.1}$$

where the wave-vectors are a function of the respective angular frequency of each photon.

The energy conservation constraint can be written in terms of the angular frequencies of the photons, ω_μ,

$$\Delta\omega = \omega_{p1} + \omega_{p2} - \omega_s - \omega_i = 0 \tag{1.2}$$

The two pump frequencies, ω_{p1} and ω_{p2}, need not be the same and can carry any value.

1.6 Outline

This thesis is presented in 4 chapters. Chapter 2 explains how birefringence is introduced in standard single mode fibers. It also describes an experimental setup that uses degenerate pump photons to generate signal and idler photon pairs in a birefringent single-mode fiber via SFWM. In chapter 3 we present a theoretical study for the generation of photon pairs in birefringent single mode fibers when the two pumps are non-degenerate. Chapter 4 summarizes the findings of this thesis.

Chapter 2

SPONTANEOUS FOUR-WAVE MIXING USING DEGENERATE PUMP PHOTONS: EXPERIMENTAL IMPLEMENTATION

This chapter examines an experimental implementation of a one-pump SFWM process in which two degenerate pump photons from a single pump generate a signal and idler photon pair in a standard birefringent fiber. The second order coherence function, $g^{(2)}$, as well as the heralding efficiency, is used to quantify the heralding correlation between the signal and idler photons.

2.1 Birefringent Standard Fibers

Media that display two different indices of refraction for two orthogonal polarizations of light are said to be birefringent. Birefringence can be seen in anisotropic materials such as calcite crystals and quartz. Glass, on the other hand, is not anisotropic; it is isotropic. In isotropic media, light behaves the same way regardless of polarization. Therefore, standard optical fibers, which are usually made of glass, are not inherently birefringent.

In standard optical fibers, birefringence can be introduced by applying an asymmetrical stress on the core of the fiber [3]. This can be done by adding rods in the cladding or by adulterating the core geometry by breaking its circular symmetry. The birefringence introduces two orthogonal axes, a fast axis and a slow axis, that have different indices of refraction, such that one polarization experiences the index of refraction of the fast axis (n_{fast}) while the orthogonal polarization experiences the slow axis index $n_{slow} > n_{fast}$.

Since the index of refraction along these axes are different, the phase velocity of the light along each axis will be different as well. The axis with the higher refractive

index (slow axis) will allow light to propagate with a slower phase velocity, while the other axis with a lower refractive index (fast axis) will allow light to propagate with a faster phase velocity. Assuming the birefringence, $\Delta n = n_{slow} - n_{fast}$, is independent of the wavelength, the effective wave-vectors of the beams polarized along the waveguide's principal fast and slow axes can be approximated [3]:

$$k_{fast}(\omega) = n_{silica}(\omega)\frac{\omega}{c} \tag{2.1}$$

$$k_{slow}(\omega) = k_{fast}(\omega) + \Delta n\frac{\omega}{c} \tag{2.2}$$

where $n_{silica}(\omega)$ is the refractive index of the angular frequency ω in bulk pure silica.

The higher the birefringence, the more strongly the fiber will preserve polarization. In this experiment, it can be assumed that the birefringence is large enough such that the polarization of light along either the fast or slow axis will be guided without varying the state of its initial polarization.

2.2 Phasematching for Degenerate Pump Photons

In order to see the effect of the birefringence on the phasematching condition for degenerate pumps, (i.e. $\omega_{p1} = \omega_{p2} = \omega_p$ and $k_{p1} = k_{p2} = k_p$), let us first look at the general phasematching and energy conservation conditions for degenerate pumps,

$$\Delta k(\omega_p, \omega_s, \omega_i) = 2k_p(\omega_p) - k_s(\omega_s) - k_i(\omega_i) = 0 \tag{2.3}$$

$$2\omega_p = \omega_s + \omega_i \tag{2.4}$$

We now assume that the pump travels along the slow axis while the signal and idler are created with orthogonal polarization, thus traveling along the fast axis. The wave-vector of the pump can be written then as:

$$k_p = k_{slow}(\omega_p) = k_{fast}(\omega_p) + \Delta n\frac{\omega_p}{c} \tag{2.5}$$

The signal and idler wave-vectors can be written as

$$k_{s,i}(\omega_{s,i}) = k_{fast}(\omega_{s,i}) \tag{2.6}$$

Therefore, when the SFWM process occurs in a birefringent standard fiber, the phase-matching condition can be written as

$$\Delta k = 2k(\omega_p) - k(\omega_s) - k(\omega_i) + 2\Delta n \frac{\omega_p}{c} \tag{2.7}$$

where $k(\omega) = k_{fast}(\omega)$ is the wave-number in pure bulk fused silica [22], whose refractive index can be calculated using the Sellmeier equation.

The Sellmeier equation is an empirical relationship between refractive index n and wavelength λ for a particular medium. In its most general form, it is:

$$n(\lambda) = \sqrt{1 + \sum_{i=1}^{m} \frac{B_i \lambda^2}{\lambda - \lambda_i}} \tag{2.8}$$

where B_i and λ_i are parameters that are experimentally obtained. For fused silica, the values of these parameters are [14],

$$\begin{aligned} B_1 &= 0.6961663 & B_2 &= 0.4079426 & B_3 &= 0.6961663 \\ \lambda_1 &= 68.4043 \text{ nm} & \lambda_2 &= 116.2414 \text{ nm} & \lambda_3 &= 9896.161 \text{ nm} \end{aligned} \tag{2.9}$$

Using the Sellmeier equation for fused silica to calculate the index (and hence the wave-number, see eq. (2.1)) of the fast axis, and assuming a birefringence $\Delta n = 4.3 \times 10^{-4}$ [22], a phase-matching plot (solution to eq. (2.7)) within the pump wavelength range of 690 - 730 nm can be generated and is shown in figure 2.1.

As can be seen, phasematching solutions exist for pump wavelengths accessible with a Ti:Sapph laser, and the signal and idler are produced in the visible range for which readily available single-photon detectors are ideal.

2.3 Experimental Setup

We generated signal and idler photon pairs via SFWM using degenerate pump photons. The experimental setup shown in figure 2.2 was used. A mode-locked femtosecond Ti:Sapph laser was used, operating at a wavelength of 715 nm with bandwidth 6 nm.

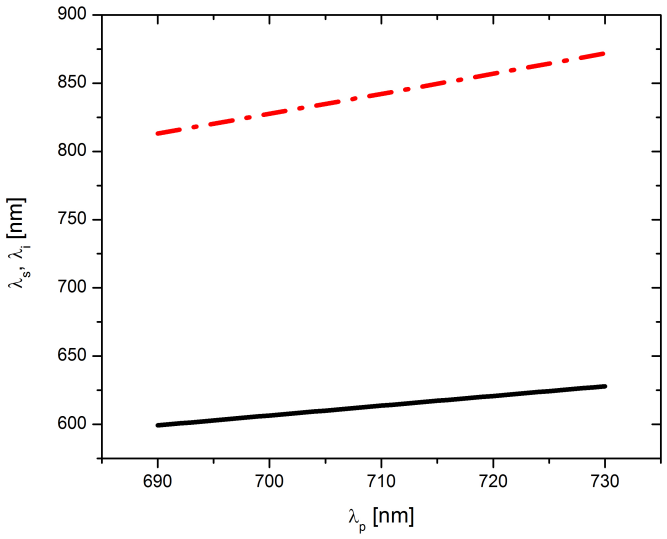

Figure 2.1: Theoretical birefringence phase-matching plot in the case of degenerate pump photons: the signal (dashed red) and idler (solid black) that satisfy eq. (2.7) with $\Delta n = 4.3 \times 10^{-4}$ as a function of the pump wavelength.

The light pulses from the laser constitute the (degenerate) pump. A half-wave plate rotates the polarization and aligns it with the slow axis of the birefringent single mode fiber (BSMF). The BSMF used is the Fibercore 800G fiber.

The power before the BSMF is 50 mW, while the power after the fiber is 25 mW (meaning that 50% of the light is coupled). As discussed above, the SFWM interaction generates photon-pairs with polarization orthogonal to the pump. The polarizer after the BSMF rejects pump light and transmits the generated signal and idler photons.

A dichroic mirror (DM) (Semrock FF685-Di02) separates the signal and idler into two arms. The reflected beam (green line in figure 2.2) corresponds to the signal photon, while the transmitted beam (yellow line) corresponds to the idler photon. The signal photon first passes through a band pass filter (BPF) (Semrock FF01-609/54), then is coupled into a multimode fiber (MMF) connected to an avalanche photo diode (APD) that detects single photons.

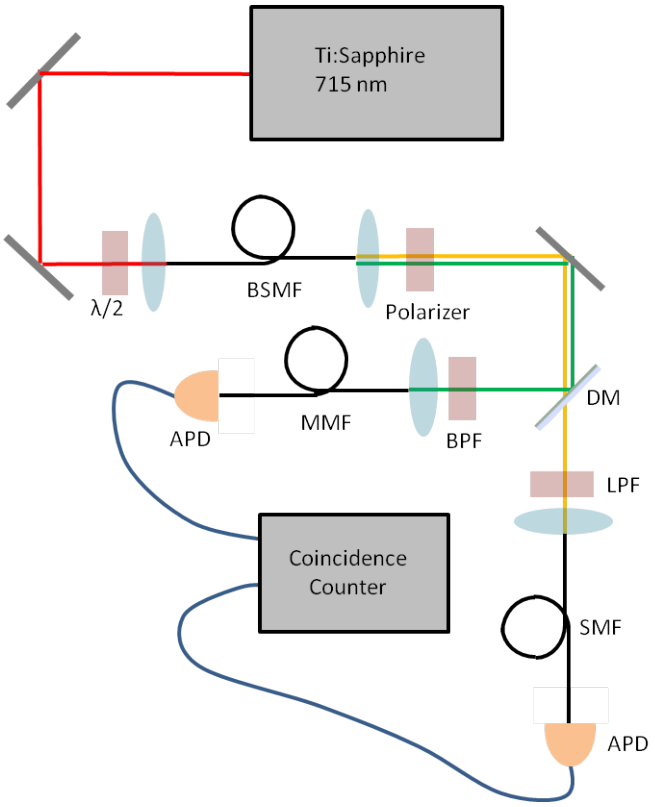

Figure 2.2: Experimental setup for detection and generation of photon pairs via SFWM in a birefringent single mode fiber (BSMF) that acts as the SFWM interaction medium. The photon pair is split into respective arms by a dichroic mirror (DM). A band pass filter (BPF) and a long pass filter (LPF) are used to filter the signal and idler, respectively. Avalanche photo diodes (APDs) collect the signal and idler photons.

The idler photon first passes through a long pass filter (LPF) (Semrock LP02-830), then through a single mode fiber (SMF) that collects well the generated idler photons and rejects most of the background noise. The SMF is then connected to an avalanche photo-diode (APD). Both APDs are connected to a coincidence counter that counts the detection events at each APD as well as the coincidence detection events.

Before checking for coincidences, we needed to ensure that we were indeed generating signal and idler photons and were able to detect them. In order to do this, the signal and idler photons were sent to a spectrometer (instead of APDs). Figure 2.3 shows the spectral measurement of the signal and idler photons.

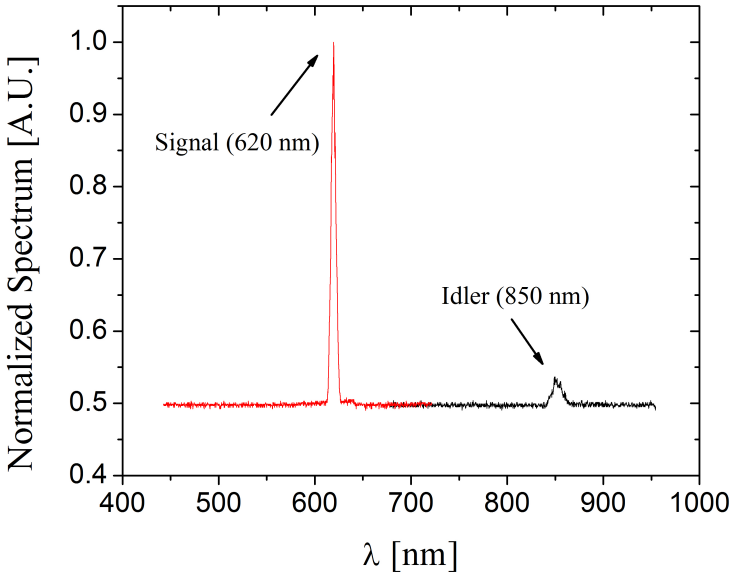

Figure 2.3: Normalized spectra of signal (red) and idler (black) photons generated in the Fibrecore 800G fiber. The pump was centered at 715 nm.

Once the signal and idler were observed on the spectrometer, the APDs were used to record the number of single photon counts of the signal and idler, as well as the number of coincidences in a 5 ns time window.

2.3.1 Second-Order Coherence Function

Suppose that for each pump pulse the probability to detect signal and idler photons is given by P_A and P_B. If these two events are uncorrelated with each other, the probability to detect a coincidence of both signal and idler is given by the product $P_A P_B$, respectively. If, however, the coincidence probability $P_{AB} > P_A P_B$, it means that a correlation between the two detection events exists. In particular, $P_{AB} > P_A P_B$ implies that the signal and idler photons are created together. In our experiment, we count events occurring during a fixed time (1 second), thus we directly measure R_x, which is the rate of event x ($x = A, B$ or AB). The probability per pump pulse P_x can be calculated by $P_x = \frac{R_x}{f}$, where f is the repetition rate of the laser (80 MHz). The

second order coherence function $g^{(2)}$ is then,

$$g^{(2)} = \frac{P_{AB}}{P_A P_B} = \frac{R_{AB}}{R_A R_B} f \tag{2.10}$$

If the value of $g^{(2)} = 1$, events A and B are independent. If $g^{(2)} > 1$, a correlation between event A and B is present. The larger the value of $g^{(2)}$, the stronger the correlation. In other words, if the value of $g^{(2)} > 1$, one can qualitatively deduce that the detection of one photon indicates, or *heralds*, the existence of the other.

We set the power before the BSMF to 21 mW and a power of 13 mW was measured after the BSMF. The number of occurrences of event A, B, and coincidence AB, during 1 second of measurement, are given by N_A, N_B, and N_{AB}, respectively. The single photon counts per second for the signal and idler were $N_B = 456,694$ and $N_A = 449,142$, respectively. The number of two-fold coincidences within a given time window of 5 ns was $N_{AB} = 92{,}962$.

The second coherence $g^{(2)}$ was measured to be $36.25 >> 1$, showing a strong pair-wise correlation between the photons.

Using the repetition rate of the laser (80 MHz), the number of photons per second is given as 8.3×10^7. From this, the efficiency of producing signal and idler photons (i.e. the number of photons per second over the number of signal/idler single counts) are 0.548% and 0.539%, respectively. We can then say that we are in the regime of single photons.

The number of counts of signal and idler photons are approximately the same; however, figure 2.3 does not show this. This is because the spectrometer was set to optimize the photon counts in the signal wavelength.

2.3.2 Heralding Efficiency

Another quantity that describes the correlations between the signal and the idler photons is the heralding efficiency, i.e. the probability to detect a signal photon

upon detection of the heralding idler, or *vice-versa*. The heralding efficiency is,

$$\text{heralding efficiency of event B} = \frac{N_{AB}}{N_A} \tag{2.11}$$

$$\text{heralding efficiency of event A} = \frac{N_{AB}}{N_B} \tag{2.12}$$

The heralding efficiency of the signal and idler were 20.7% and 20.4%, respectively. The 5 ns window is chosen such that it is shorter than the repetition rate of the laser, which at 80 MHz corresponds to a 12.5 ns time difference between laser pulses. This ensures that the coincidences recorded are pair-produced by a single laser pulse. These heralding efficiencies are reasonable, considering typical detector efficiencies of ~ 50 % and optical losses.

Both the heralding efficiency and the second order coherence function were measured by using a LabView program coupled with a coincidence counter.

Chapter 3

SPONTANEOUS FOUR-WAVE MIXING USING NON-DEGENERATE PUMP PHOTONS: A THEORETICAL STUDY

This chapter presents a theoretical study of the spontaneous four-wave mixing process with non-degenerate pump photons, i.e. we assume that *two* pump pulses with *different* central wavelengths are sent into the fiber. The SFWM process studied here assumes that one photon from *each* pump is annihilated and signal and idler photons are created. Specifically, we are interested in the degree to which the signal and idler photons are uncorrelated, which, as will be explained, is particularly important for the heralding of a single photon in a pure wave-packet, and hence for many quantum technology applications, including LOQC. We first discuss the phasematching conditions for this case and compare it with the degenerate pump case. We then investigate the joint spectral properties of the signal and idler photons, using theoretical and numerical calculations.

3.1 Phasematching for Non-Degenerate Pump Photons

When we consider the SFWM interaction that includes non-degenerate pumps, the phasematching and energy conservation conditions are

$$\Delta k(\omega_{p1}, \omega_{p2}, \omega_s, \omega_i) = k_{p1}(\omega_{p1}) + k_{p2}(\omega_{p2}) - k_s(\omega_s) - k_i(\omega_i) = 0 \tag{3.1}$$

$$\Delta\omega = \omega_{p1} + \omega_{p2} - \omega_s - \omega_i = 0 \tag{3.2}$$

Where p_1 and p_2 represent pump 1 and pump 2, respectively, while the subscripts s and i represent the signal and idler. Similar to the degenerate case, we include the birefringence of the fiber and assume that both pump pulses are polarized along the principal slow axis of the fiber, while the generated signal and idler are polarized along

the fast axis of the fiber. Assuming again that the wave-number $k(\omega)$ for light polarized along the fast axis is given by the wave-number in bulk fused silica, the phasematching and energy conservation conditions become

$$\Delta\omega = \omega_{p1} + \omega_{p2} - \omega_s - \omega_i = 0 \tag{3.3}$$

$$\Delta k = k(\omega_{p1}) + k(\omega_{p2}) - k(\omega_s) - k(\omega_i) + \Delta n \frac{\omega_{p1} + \omega_{p2}}{c} = 0 \tag{3.4}$$

We define the "average" wavelength $\lambda_p = 2\pi c/\omega_p$ where $\omega_p = (\omega_{p1} + \omega_{p2})/2$ is the mean frequency of the two pumps, and c is the speed of light in free space. We also define the wavelength detuning $\Delta\lambda = \lambda_{p1} - \lambda_p$ where $\lambda_{p1} = 2\pi c/\omega_{p1}$ is the vacuum wavelength of pump 1. Similarly, λ_{p2} is the vacuum wavelength of pump 2.

Figure 3.1 shows the phase-matching contour plot (i.e. solutions to eq. (3.4)) versus the average wavelength of the pumps, λ_p, for different values of the detuning, $\Delta\lambda$.

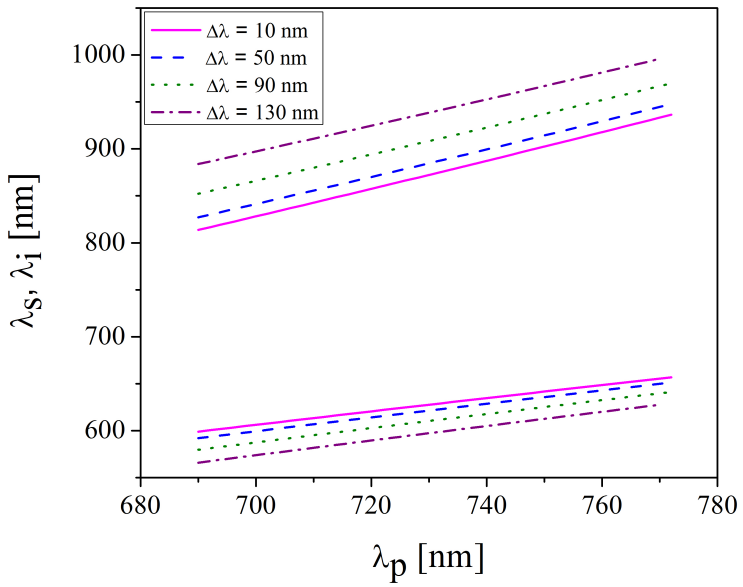

Figure 3.1: Theoretical birefringent phase-matching contour as a function of the pumps' average wavelength, λ_p, with various values for detuning, $\Delta\lambda$. The birefringence is $\Delta n = 4.3 \times 10^{-4}$.

3.2 Joint Spectral Amplitude

The general form of a photon-pair state for the signal and idler modes is [17],

$$|\Psi\rangle = \int\int d\omega_s d\omega_i f(\omega_s, \omega_i)|\omega_s\rangle_s|\omega_i\rangle_i \tag{3.5}$$

where $f(\omega_s, \omega_i)$ is the joint spectral amplitude of the signal and the idler. $|\omega_s\rangle_s|\omega_i\rangle_i$ is the two-photon state with frequencies ω_s and ω_i.

In the case of SFWM, the joint spectrum of the generated photon pair can be written as [3],

$$f(\omega_s, \omega_i) = N \int d\omega_{p1} e^{-i\omega_{p1}\tau} e^{-\left(\frac{\omega_{p1}-\omega_{p1}^0}{\sigma_{p1}}\right)^2} e^{-\left(\frac{\omega_s+\omega_i-\omega_{p1}-\omega_{p2}^0}{\sigma_{p2}}\right)^2} \int_0^L dz e^{-i\Delta k z} \tag{3.6}$$

where N is a normalization constant, τ is a time delay (possibly) applied to pump 1 relative to pump 2, L is the length of the fiber, σ_{p1} and σ_{p2} are the bandwidths of pump 1 and 2, respectively, Δk is the wave-vector mismatch given by (3.4), and ω_{p1}^0 and ω_{p2}^0 are the central angular frequencies of the pumps. Integrating over z, the joint spectrum is

$$f(\omega_s, \omega_i) = N \int d\omega_{p1}\ \mathrm{sinc}\left(\frac{L\Delta k}{2}\right) e^{\frac{-iL\Delta k}{2}} e^{-i\omega_{p1}\tau} e^{-\left(\frac{\omega_{p1}-\omega_{p1}^0}{\sigma_{p1}}\right)^2} e^{-\left(\frac{\omega_s+\omega_i-\omega_{p1}-\omega_{p2}^0}{\sigma_{p2}}\right)^2} \tag{3.7}$$

Assuming that there exists some signal and idler frequencies, ω_s^0 and ω_i^0 (for given pump frequencies ω_{p1}^0 and ω_{p2}^0), such that momentum conservation and energy conservation are met, namely,

$$\Delta k(\omega_{p1}^0, \omega_{p2}^0, \omega_s^0, \omega_i^0) = 0 \tag{3.8}$$

$$\Delta\omega = \omega_{p1}^0 + \omega_{p2}^0 - \omega_s^0 - \omega_i^0 = 0 \tag{3.9}$$

It is useful to define a detuning from these frequencies, given by,

$$\nu_s = \omega_s - \omega_s^0 \tag{3.10}$$

$$\nu_i = \omega_i - \omega_i^0 \tag{3.11}$$

In order to perform the integral in eq. (3.7), it is convenient to apply the integration transformation,

$$\Omega = \omega_{p1} - \omega_{p1}^0 - \frac{\nu_s + \nu_i}{2} \tag{3.12}$$

From this integration transformation, we can find an expression containing $\omega_{p2} - \omega_{p2}^0$ by

$$\Omega = \omega_{p1} - \omega_{p1}^0 - \frac{\nu_s + \nu_i}{2} - \frac{\nu_s + \nu_i}{2} + \frac{\nu_s + \nu_i}{2} \tag{3.13}$$

$$\Omega = \omega_{p1} - \omega_{p1}^0 - (\nu_s + \nu_i) + \frac{\nu_s + \nu_i}{2} \tag{3.14}$$

$$\Omega = -(\omega_{p2} - \omega_{p2}^0) + \frac{\nu_s + \nu_i}{2} \tag{3.15}$$

where $\omega_{p2} = \omega_s + \omega_i - \omega_{p1}$.

The wave-vector mis-match, Δk, can now be approximated to first order using a Taylor expansion,

$$\Delta k \approx \frac{1}{L}(\nu_s \tau_s + \nu_i \tau_i + \tau_p \Omega) \tag{3.16}$$

where

$$\tau_i = L\left(\frac{k'_{p1}(\omega_{p1}^0) + k'_{p2}(\omega_{p2}^0)}{2} - k'_i(\omega_i)\right) \tag{3.17}$$

and

$$\tau_p = L\left(k'_{p1}(\omega_{p1}^0) - k'_{p2}(\omega_{p2}^0)\right) \tag{3.18}$$

$$k'_\mu(\omega_\mu^0) = \left.\frac{dk_\mu}{d\omega}\right|_{\omega=\omega_\mu^0} \text{ for } \mu = p_1, p_2, s, i \tag{3.19}$$

τ_p is the group delay between the two pumps that is introduced during propagation in the fiber. Note that since we consider the two pumps to be centered at different wavelengths, their group velocities can differ and therefore $\tau_p \neq 0$. This is a major difference with the degenerate pump case, where both pump photons that interact through SFWM travel at the same velocity since they are provided by the same pump field. We have also defined

$$\tau_s = \frac{\tau_{s1} + \tau_{s2}}{2} = L\left(\frac{k'_{p1}(\omega_{p1}^0) + k'_{p2}(\omega_{p2}^0)}{2} - k'_s(\omega_s)\right) \tag{3.20}$$

as the average group delay between the signal and pump 1 ($\tau_{s1} = L(k'_{p1}(\omega^0_{p1}) - k'_s(\omega_s))$) and the signal and pump 2 ($\tau_{s2} = L(k'_{p2}(\omega^0_{p2}) - k'_s(\omega_s))$) during propagation in the fiber. A similar expression can be written for the idler.

The first-order Taylor approximation (eq. (3.16)) for Δk can be applied when the modes involved in the SFWM interaction experience a negligible dispersion [3]. With this approximation, as well as the appropriate substitutions, the joint spectral amplitude, eq. (3.7), now in terms of ν_s and ν_i, can be written as:

$$\begin{aligned} F(\nu_s,\nu_i) = N\ & e^{-i\frac{1}{2}\nu_s\tau} e^{-i\frac{1}{2}\nu_i\tau} e^{-i\tau\omega^0_{p1}} e^{-i\frac{1}{2}(\nu_s\tau_s+\nu_i\tau_i)} \times \\ & \int d\Omega\ \mathrm{sinc}\left(\frac{1}{2}(\nu_s\tau_s+\nu_i\tau_i)+\frac{1}{2}\Omega\tau_p\right) e^{-i\frac{1}{2}\Omega\tau_p} e^{-i\Omega\tau} \times \\ & e^{-\left(\frac{\frac{\nu_s+\nu_i}{2}+\Omega}{\sigma_{p1}}\right)^2 - \left(\frac{\frac{\nu_s+\nu_i}{2}-\Omega}{\sigma_{p2}}\right)^2} \end{aligned} \tag{3.21}$$

Performing the integral, one is left with the following expression for the joint spectrum,

$$\begin{aligned} F(\nu_s,\nu_i) = N\pi^{\frac{3}{2}} \frac{\sigma_1\sigma_2}{\sigma\tau_p} \frac{1}{\sqrt{\sigma_1^2+\sigma_2^2}}\ & e^{-i(\frac{1}{2}(\nu_s\tau_s+\nu_i\tau_i)+\omega^0_{p1}\tau+(\frac{\nu_s+\nu_i}{2})\tau)} e^{-\left[\frac{1}{\sigma^2}+\frac{\sigma^2}{\Sigma^2}\right]\left(\frac{\nu_s+\nu_i}{2}\right)^2} \\ & e^{it\frac{\nu_s\tau_s+\nu_i\tau_i}{\tau_p}} e^{-\frac{1}{\sigma^2}\left(\frac{\nu_s\tau_s+\nu_i\tau_i}{\tau_p}\right)^2 + \left(\frac{\sigma^2}{\Sigma^2}\left(\frac{\nu_s+\nu_i}{2}\right)\right)^2 + \frac{\sigma^2}{\Sigma^2}(\nu_s+\nu_i)} \\ & \times \mathrm{erf}\left(\frac{\sigma(\tau_p+\tau)}{2} + i\frac{T_s\nu_s+T_i\nu_i}{\sigma\tau_p}\right) - \mathrm{erf}\left(\frac{\sigma\tau}{2} + i\frac{T_s\nu_s+T_i\nu_i}{\sigma\tau_p}\right) \end{aligned} \tag{3.22}$$

Where T_s, T_i, σ, and Σ are defined as

$$T_\mu = \tau_\mu + \frac{\sigma^2}{2\Sigma^2}\tau_p = \tau_\mu + \frac{1}{2}\frac{\sigma_1^2-\sigma_2^2}{\sigma_1^2+\sigma_2^2}\tau_p \tag{3.23}$$

$$\sigma = \frac{\sigma_1\sigma_2}{\sqrt{\sigma_1^2+\sigma_2^2}} \tag{3.24}$$

$$\Sigma = \frac{\sigma_1\sigma_2}{\sqrt{\sigma_1^2-\sigma_2^2}} \tag{3.25}$$

for $\mu = s, i$. Two functions can now be defined:

$$\alpha(\nu_s,\nu_i) = \frac{1}{\sqrt{\sigma_1^2+\sigma_2^2}}\left[e^{-\frac{(\nu_s+\nu_i)^2}{\sigma_1^2+\sigma_2^2}}\right] \tag{3.26}$$

The above function, $\alpha(\nu_s, \nu_i)$, is called the pumps' envelope function and accounts for the energy conservation constraint only and depends on the pumps' spectral envelope, but not on the fiber characteristics. The function

$$\Phi(\nu_s, \nu_i) = \frac{\sigma_1 \sigma_2}{\sigma \tau_p} e^{-\left(\frac{T_s \nu_s + T_i \nu_i}{\sigma \tau_p}\right)^2} \times \left[\text{erf}\left(\frac{\sigma(\tau_p + \tau)}{2} + i \frac{T_s \nu_s + T_i \nu_i}{\sigma \tau_p} \right) - \text{erf}\left(\frac{\sigma \tau}{2} + i \frac{T_s \nu_s + T_i \nu_i}{\sigma \tau_p} \right) \right] \tag{3.27}$$

is called the phasematching function, and expresses the phasematching (momentum conservation) constraints and depends on the dispersion in the fiber (through τ_p, τ_s and τ_i). The joint spectrum can finally be written as:

$$F(\nu_s, \nu_i) = N \pi^{\frac{3}{2}} e^{-i\omega_{p1}^0 \tau} e^{i \frac{\tau}{\tau_p} (\tau_s \nu_s + \tau_i \nu_i)} \alpha(\nu_s, \nu_i) \Phi(\nu_s, \nu_i) \tag{3.28}$$

Further details about the calculation for the joint spectral amplitude for non-degenerate pumps can be found in the appendix.

Using the expression for the joint spectrum, eq. (3.28), a plot of the joint spectral amplitude can then be generated, shown in figure 3.2. The error function in the phase-matching function, $\Phi(\nu_s, \nu_i)$, is evaluated numerically.

3.3 Interaction in the Fiber

The SFWM interaction takes place only if the two pump pulses overlap in the fiber. Therefore, in this thesis, we set the value of τ to be $\tau = -\frac{1}{2}\tau_p$. This means that the pump with greater group velocity (in the fiber) is delayed relative to the other pump such that it catches up with the slower pump at the center of the fiber, and then leaves the slower pump behind. These settings guarantee maximal interaction duration in the fiber.

The result of the joint spectrum, (3.22), can be further investigated by finding analytical expressions in two regimes. The first regime is one where the temporal walk-off between the two pump beams is negligible (compared to the duration of the pulsed pumps). In this case, the two pump beams are overlapped for the full length

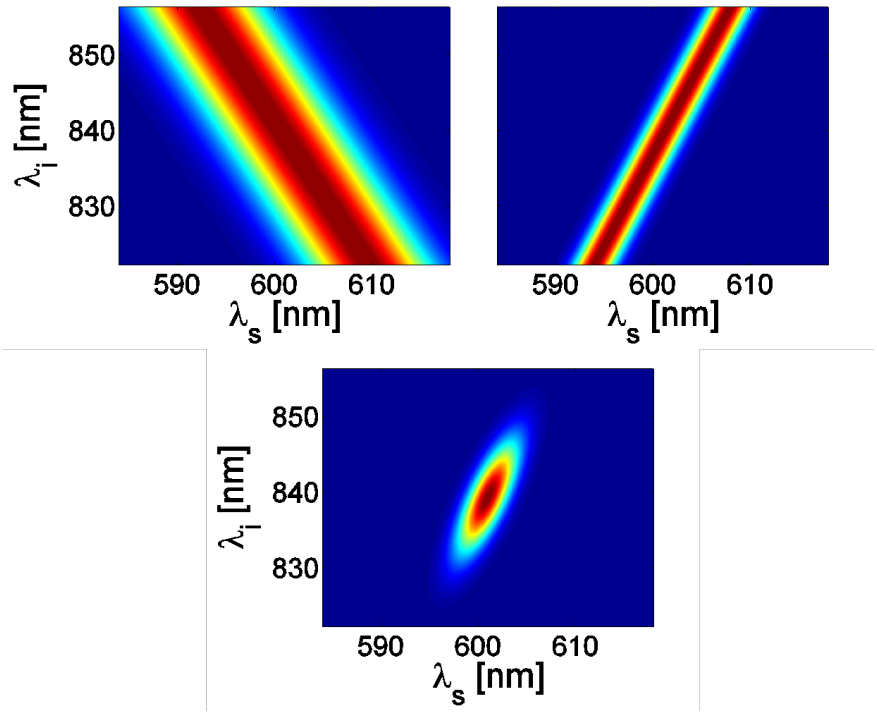

Figure 3.2: Energy conservation, $|\alpha(\nu_s, \nu_i)|^2$ (top left) and phase-matching, $|\Phi(\nu_s, \nu_i)|^2$ (top right) functions for $\lambda_p = 700$ nm and $\Delta\lambda = 45$ nm. Their product (bottom) is the joint spectral amplitude, $|F(\nu_s, \nu_i)|^2$, as given in eq. (3.22). The bandwidths of the two pumps is $\sigma_1 = \sigma_2 = 5$ nm. Length of the fiber is 0.1 m

of the fiber and thus the SFWM interaction turns on and off abruptly upon the pulses entering and exiting the fiber. This situation can be described as one which satisfies the following condition: $|\sigma\tau_p| << 1$.

In the opposite regime, $|\sigma\tau_p| >> 1$, the pump with the slower group velocity is sent well ahead of the second pump pulse such that there is no temporal overlap between the pumps upon entering the fiber. The fiber is long enough such that the faster pump catches up with the slower pump at the center of the fiber, and the two interact fully. The two then are separated completely due to their difference in group velocities, such that when they exit the fiber, there is no spatial overlap between the two pump pulses.

3.3.1 Regime 1: negligible temporal walk-off between the two pump beams ($|\sigma\tau_p| << 1$)

In this regime it can be shown that the joint spectral amplitude can be evaluated to (recalling that $\tau = -\tau_p/2$)

$$F(\nu_s, \nu_i) = N\pi^{\frac{3}{2}} e^{-i\omega_{p1}^0 \tau} e^{-i\frac{1}{2}\nu_s \tau} e^{-i\frac{1}{2}\nu_i \tau} e^{i\frac{\tau}{\tau_p}(\nu_s \tau_s + \nu_i \tau_i)} \alpha(\nu_s, \nu_i)\phi(\nu_s, \nu_i) \tag{3.29}$$

where

$$\alpha(\nu_s, \nu_i) = \frac{1}{\sqrt{\sigma_1^2 + \sigma_2^2}} e^{-\frac{(\nu_s+\nu_i)^2}{\sigma_1^2+\sigma_2^2}} \tag{3.30}$$

$$\phi(\nu_s, \nu_i) = e^{-i\frac{T_s\nu_s + T_i\nu_i}{2}} \operatorname{sinc}\left(\frac{T_s\nu_s + T_i\nu_i}{2}\right) \tag{3.31}$$

Using the general equation for the joint spectrum (3.28), a plot of the joint spectrum can be generated in this regime, as seen in figure 3.3. It can be seen that in addition to the central lobe, side lobes are present. These lobes are related to the wings of the sinc function, and appear because of the abrupt nature of the interaction: the interaction starts abruptly when the pumps enter the fiber, takes place throughout the fiber and stops abruptly once the pumps exit the fiber.

It should be noted that in the case of degenerate pumps the "two" pump pulses travel at the same group velocity, and $\sigma\tau_p = 0$ (because $\tau_p = 0$). Hence this case falls under the $\sigma\tau_p << 0$ condition. Also, in this case $\sigma_{p1} = \sigma_{p2}$, and $T_s = \tau_s$, $T_i = \tau_i$ and $\sigma = \frac{\sigma_p}{\sqrt{2}}$, where σ_p is bandwidth of pump pulses. In the $|\sigma\tau_p| << 1$ regime for non-degenerate pumps the joint spectral amplitude is identical in form to the degenerate pump case. The latter has already been studied extensively [13, 17, 22] in various configurations, and as mentioned, those results are valid for the non-degenerate pumps with negligible temporal walk-off. We therefore concentrate on a different regime where the temporal walk-off between the pumps is appreciable.

3.3.2 Regime 2: $|\sigma\tau_p| >> 1$

This regime describes the situation where the slower pump is sent well before the faster pump such that there is no temporal overlap between the two pumps at

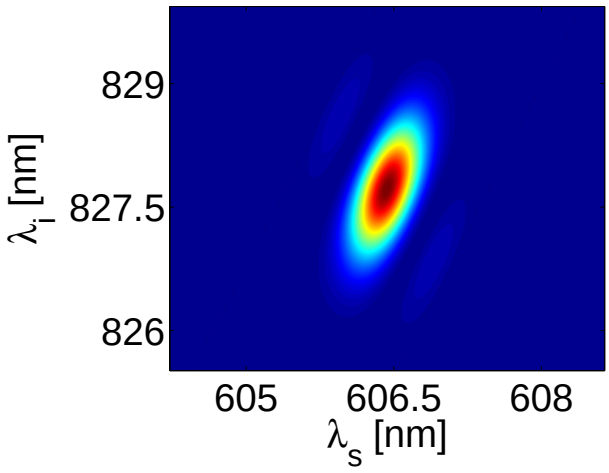

Figure 3.3: Calculated Joint spectral amplitude for the parameters $\lambda_p = 700$ nm, length of fiber = 0.1 m, $\sigma_{p1} = \sigma_{p2} = 0.52$ nm. The value for $|\sigma\tau_p|$ is 0.4118. The birefringence, $\Delta n = 4.3 \times 10^{-4}$.

the beginning ($|\sigma\tau| = (1/2)|\sigma\tau_p| >> 1$). The faster pump then catches up to the slower pump, resulting in an interaction within the fiber. The fiber is long enough such that the faster pump completely overtakes the other and there is no temporal overlap between the two pump beams upon exiting the fiber ($|\sigma\tau_p| >> 1$). It can be shown that these assumptions simplify the joint spectral amplitude to

$$F(\nu_s, \nu_i) = \left[N\pi^{\frac{5}{2}} \frac{\sigma_1\sigma_2}{|\sigma\tau_p|} e^{-i\omega_{p1}^0\tau} e^{-i\frac{1}{2}\nu_s\tau} e^{-i\frac{1}{2}\nu_i\tau} e^{i\frac{\tau}{\tau_p}(\nu_s\tau_s+\nu_i\tau_i)} \right] \alpha(\nu_s, \nu_i)\phi(\nu_s, \nu_i) \tag{3.32}$$

where

$$\alpha(\nu_s, \nu_i) = \frac{1}{\sqrt{\sigma_1^2 + \sigma_2^2}} e^{-\frac{(\nu_s+\nu_i)^2}{\sigma_1^2+\sigma_2^2}} \tag{3.33}$$

$$\phi(\nu_s, \nu_i) = e^{-\left(\frac{T_s\nu_s+T_i\nu_i}{\sigma\tau_p}\right)^2} \tag{3.34}$$

Figure 3.4 shows an example of the joint spectrum in this regime. There are no side lobes present in this case, because unlike in the previous regime, the interaction happens gradually as the fast pump crosses over the slow one, and the phase-matching function, $\phi(\nu_s, \nu_i)$, is described as a Gaussian as opposed to a sinc function in the previous regime (the latter is responsible for the side-lobes in figure 3.3).

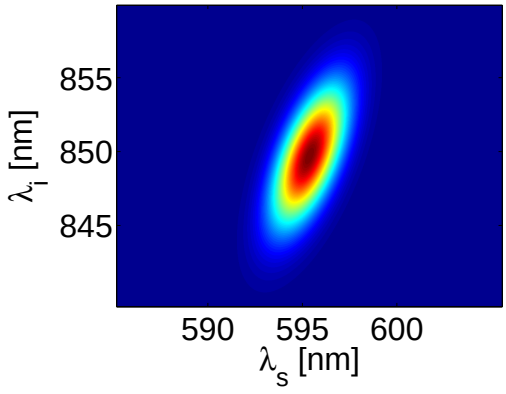

Figure 3.4: Joint spectral amplitude in the regime $|\sigma\tau_p| >> 1$, given the parameters: central wavelength $\lambda_p = 700$ nm, detuning $\Delta\lambda = 65$ nm, L = 0.1 m, $\sigma_{p1} = \sigma_{p2} = 3$ nm, $|\sigma\tau_p|$ is 28.43. Note that no side lobes are present here (compare with figure 3.3).

3.4 Purity and Factorability

The joint spectral amplitude encompasses spectral correlations between the signal and idler photons. Due to energy and momentum conservation constraints, these correlations are usually strong (see for example figures 3.3 and 3.4), i.e., any knowledge gained about the signal spectrum gives away information about the idler, and *vice-versa*. As we explain below, if we detect one of the photons to herald the other, the resultant heralded photon is in a mixed state, rather than pure, and is therefore rendered useless for the LOQC protocol. In order to use the photons in the LOQC scheme, the generated photons must be uncorrelated (and then the heralded photon is pure). The purity of each individual photon in the photon pair quantifies the strength of the correlations between them.

Let's look again at the general form of a photon-pair state,

$$|\Psi\rangle = \int\int d\omega_s d\omega_i f(\omega_s, \omega_i)|\omega_s\rangle_s|\omega_i\rangle_i \tag{3.35}$$

According to the Schmidt-decomposition procedure, the state of the photon pair can

be written as,

$$|\Psi\rangle = \sum_n \sqrt{\lambda_n}|s_n\rangle|i_n\rangle \tag{3.36}$$

where the Schmidt coefficients, λ_n, are non-negative numbers satisfying $\sum_n \lambda_n = 1$, and $\{|s_n\rangle\}$ and $\{|i_n\rangle\}$ are orthonormal states representing the signal and idler photons. The density matrix associated with $|\Psi\rangle$ is

$$\rho = |\Psi\rangle\langle\Psi| = \sum_{nm} \sqrt{\lambda_n\lambda_m}|s_n\rangle\langle s_m| \otimes |i_n\rangle\langle i_m| \tag{3.37}$$

Tracing over the signal degrees of freedom we obtain the individual idler density matrix π_i, or tracing over the idler degrees of freedom we obtain the signal density matrix π_s:

$$\pi_i = Tr_s[\rho] = \sum_n \lambda_n|i_n\rangle\langle i_n| \tag{3.38}$$

$$\pi_s = Tr_i[\rho] = \sum_n \lambda_n|s_n\rangle\langle s_n| \tag{3.39}$$

Generally, the above density matrices represent signal and idler in mixed states. In order to use the signal and idler photons for LOQC schemes, the signal and idler photons must be in a pure state, in which case, they are uncorrelated, resulting in a joint spectral amplitude

$$f(\omega_s, \omega_i) = S(\omega_s)I(\omega_i) \tag{3.40}$$

where $S(\omega_s)$ is independent of the idler frequencies and I(ω_i) is independent of the signal frequency. In this case, the joint spectrum is factorable. The purity, which quantifies the factorability of the joint spectrum, is given by

$$p = Tr[\pi_s^2] = Tr[\pi_i^2] = \sum_n \lambda_n^2 \tag{3.41}$$

For pure photons, the purity, $p = 1$. As the purity decreases to 0, the photons' state becomes more mixed. Using the joint spectral amplitude, $f(\omega_s, \omega_i)$, the purity is evaluated as

$$p = \int f(\omega_1, \omega_2)f^*(\omega_3, \omega_2)f(\omega_3, \omega_4)f^*(\omega_1, \omega_4)d\omega_1 d\omega_2 d\omega_3 d\omega_4 \tag{3.42}$$

3.5 Numerical Methods

In this section we use numerical methods to evaluate the purity of generated photons. We concentrate on the regime in which $|\sigma\tau_p| >> 1$. This regime, which makes use of the group velocity difference between two pumps at different frequencies, is distinct from the well-studied degenerate pumps configuration [13, 17, 22]. Specifically, the value of $|\sigma\tau_p|$ was chosen to be 6, which means that the two (Gaussian) pumps are sent into the fiber with a time delay equal to 3 times their duration (and hence they are practically non-overlapping). The fast pump then gets closer, crosses and overtakes the slower one. When the pump beams exit the fiber, their relative delay again reaches 3 times the duration of the pulses (and hence again, practically non-overlapping). The value of $|\sigma\tau_p|$ can be modified by changing the fiber length. In essence, extending the fiber length (and thus $|\sigma\tau_p|$) in the regime $|\sigma\tau_p| >> 1$ does not affect the joint spectral amplitude (or purity), because the interaction only occurs when the two pumps overlap at the center of the fiber. We numerically confirmed that $|\sigma\tau_p| = 6$ satisfies this condition and the purity does not change by more than 1% when lengthening the fiber.

Figure 3.5 shows the joint spectral probability for values of $\Delta\lambda = 50$ nm, 150 nm, and 240 nm, as given in eq. (3.22) in the regime where $|\sigma\tau_p| >> 1$, specifically where $|\sigma\tau_p| = 6$.

The bandwidths of the two pumps were set to $\sigma_{p1} = \sigma_{p2} = 0.25$ nm. The length of the fiber for each detuning was chosen such that $|\sigma\tau_p| = 6$. For $\Delta\lambda = 50$ nm, 150 nm, and 240 nm, the fiber lengths were 32.26 cm, 12.23 cm, and 8.5 cm, respectively. The purity was also calculated for each case and is 69.96%, 96.48%, and 98.91%, respectively.

Figure 3.6 shows purity as a function of the detuning, $\Delta\lambda$, between the two non-degenerate pumps, with a central wavelength of 700 nm (black squares). As the detuning increases, the purity approaches 100%. For a central wavelength of 700 nm, the largest detuning considered was $\Delta\lambda = 240$ nm. This point yields a purity of 98.91%.

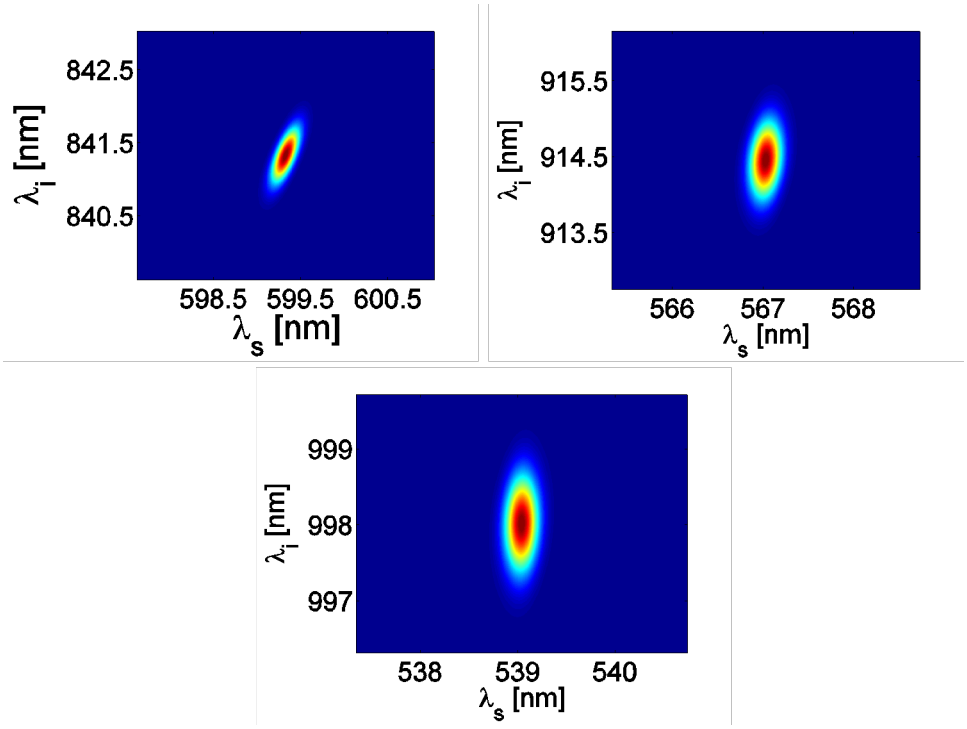

Figure 3.5: Joint spectral probability for $\Delta\lambda = 50$ nm (top left), 150 nm (top right), and 240 nm (bottom) with central wavelength $\lambda_p = 700$ nm. The bandwidths of the two pumps were $\sigma_{p1} = \sigma_{p2} = 0.25$ nm. The length of the fiber was chosen such that $|\sigma\tau_p| = 6$ and is 32.26 cm, 12.23 cm, and 8.5 cm for $\Delta\lambda = 50$ nm, 150 nm, and 240 nm, respectively. The purity for each detuning is 69.59% ($\Delta\lambda = 50$nm), 96.48% ($\Delta\lambda = 150$ nm), and 98.91% ($\Delta\lambda = 240$ nm).

As the above result is seemingly promising, we looked into the minimum frequency difference between the signal or idler and one of the pumps, namely, $\min\{|f_{p1} - f_s|, |f_{p1} - f_i|\}$ which we will call Δf. It is important to look into the relationship between Δf and $\Delta\lambda$ because processes other than SFWM occur in the fiber, including spontaneous Raman scattering. The pump field can induce spontaneous Raman scattering and generate photons shifted to the red of the pump wavelength, thus adding background at wavelengths that are shifted from the pump by up to 40Thz [19]. Because of this, it is desirable to have a large detuning between the generated photons and the pump, such that Raman contamination is small or negligible.

For each data point in figure 3.6 we also show the detuning between the photons

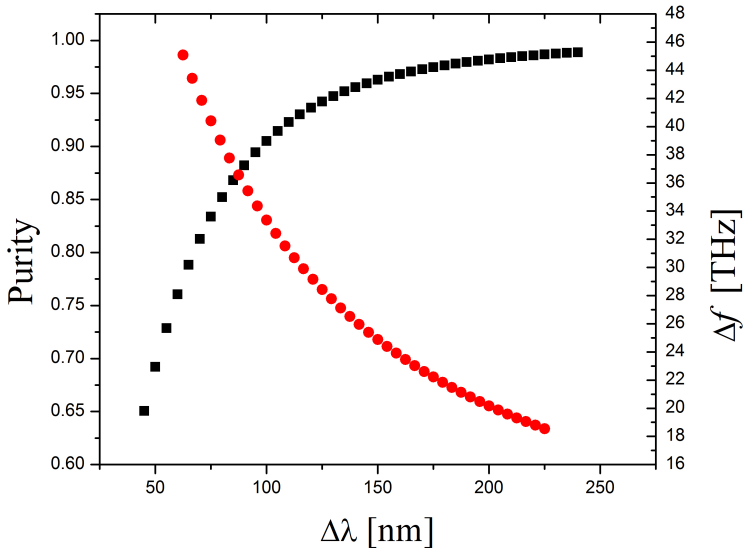

Figure 3.6: Purity (black squares) and $\min\{|f_{p1} - f_s|, |f_{p1} - f_i|\}$, Δf, (red circles) as a function of detuning, $\Delta\lambda$ in the regime where $|\sigma\tau_p| >> 1$, namely, $|\sigma\tau_p| = 6$. The time delay between the two pumps is $\tau = -\frac{1}{2}\tau_p$. The value for the central wavelength, $\lambda_p = 700$ nm.

and pump, Δf (red circles). As $\Delta\lambda$ increases, phasematching conditions impose a decrease in Δf. Thus, we approach unit purity when Δf approaches zero, resulting in signal and idler wavelengths that are identical to the two pumps. In this case, the signal and idler photons are indistinguishable from the pump photons. This validates the simplified result of (3.32). Due to numerical limitations that arose from numerically evaluating the error function, it was not possible to obtain results for values of Δf less than around 18 THz.

Chapter 4

SUMMARY

Processes that generate photon pairs simultaneously have been the most utilized heralded sources for single photons. There is a variety of media that support SPDC or SFWM processes, and the choice of the medium is often dictated by the intended application for the produced photons. In this thesis we investigated a recently discovered source of photon pairs the birefringent single-mode fiber. The creation of photons in such a fiber is motivated by the fact that their mode is matched for coupling into quantum information fiber networks that are composed of similar fibers. We experimentally confirmed that photon pairs could be generated through this type of fiber, using degenerate pumps. We then studied theoretically the spectral correlations introduced between the photons when they are created by two pump pulses with different wavelengths. We found that the group velocity difference between the two pumps can be utilized to switch the SFWM interaction on and off gradually, and showed that this feature can be employed for the creation of 100% uncorrelated photon pairs, which is a necessary condition for the heralding of pure single photons.

4.1 Conclusion

In chapter 1, we presented the motivation for this thesis: photon sources that produce pure and indistinguishable photons are necessary for the implementation of the so-called LOQC scheme. We described single photon sources, as well as the most common method to produce single photons to date, heralding. In the case of heralded photons, the photon pairs are usually in a mixed state and are not applicable for the LOQC scheme. We also discuss standard fibers and the step-index model.

In chapter 2, we described a source that produced photon pairs via the SFWM interaction in a standard optical fiber. We described an experimental implementation of a single-pump SFWM interaction. We were able to generate photon pairs such that one indeed heralded the other. We quantified the strength of the heralding correlations by the second order coherence function as well as the heralding efficiency. Both quantities showed that there was a strong pair- wise correlation between the photons.

Chapter 3 described theoretical calculations used to investigate a SFWM interaction consisting of two non-degenerate pumps by use of the joint spectral amplitude of the generated photon pair. We found that for non-degenerate pump photons, in the regime where the temporal walk-off between the two pumps is negligible, the joint spectral amplitude is identical in form to that of a SFWM interaction consisting of degenerate pumps. In this regime, the phase-matching function is that of a sinc function.

In the second regime, there was no spatial overlap between the two pumps in the beginning of the fiber. The slower pump was sent first, followed by the faster pump some time τ later. The two pumps interact in the fiber and then are separated by the difference in group velocities such that there is no interaction in the fiber upon exiting. We found that the phase-matching function was described by a Gaussian. We were also able to tailor the dispersion characteristics and conditions such that we observed photons whose purity approached unity, although at the expense of contamination due to other nonlinear processes, including Raman scattering.

Finally, in this chapter, we concluded the findings of this thesis.

BIBLIOGRAPHY

[1] D. deutsch, *Quatum Theory, the Church-Turing Principle and the Universal Quanum Computer* Royal Society of London Proceedings Series A, **400**, pp. 97 - 117 (1985).

[2] P. M. Shor, *Algorithms for Quantum Computation: Discrete Algorithms and Factoring*, in *35th Annual Symposium on Foundations of Computer Science* pp. 124 - 134 (1994).

[3] O. Cohen, *Generation of Uncorrelated Photon-Pairs in Optical Fibres*, Doctoral dissertation, Oxford University. Retrieved from Oxford University Research Archive, http://ora.ox.ac.uk/objects/uuid:b818b08a-27b5-4296-9f89-befec30b71fc.

[4] E. Knill, R. Laflamme, and G. J. Milburn, *A Scheme for Efficient Quantum Computation with Linear Optics*, Nature, **409**, pp. 46 - 52 (2001).

[5] B. Julsgaard, J. Sherson, J. I. Cirac, J. Fiurasek, and E. S. Polzik, *Experimental Demonstration of Quantum Memory for Light*, Nature, **432**, pp. 482486 (2004).

[6] S. Takeuchi, J. Kim, Y. Yamamoto, and H. H. Hogue, *Development of a Highquantum- Efficiency Single-Photon Counting System*, Applied Physics Letters, **74**, pp. 10631065 (1999)

[7] C. K. Hong, Z. Y. Ou, *Measurement of Subpicosecond Time Intervals between Two Photons by Interference*, Phys. Rev. Lett. **59**, pp. 2044 (1987).

[8] R. Loudon, *The Quantum Theory of Light*, Oxford University Press, 3rd. Edition, (2000).

[9] M. Hijlkema, B. Weber, H. P. Specht, S. C. Webster, A. Kuhn, and G. Rempe, *A Single-Photon Server With Just One Atom*, Nature Phys, **3**, pp. 253 - 255 (2007).

[10] C. Brunel, B. Lounis, P. Tamarat, and M. Orrit, *Triggered Source of Single Photons Based on Controlled Single Molecule Flourescence*, Phys. Rev. Lett. **83**, pp. 2722 - 2725 (1999).

[11] A. M. Boiron, B. Lounis, and M. Orrit *Single Molecules of Dibenzanthanthrene in n-hexadecane*, J. Chem. Phys. **105**, 3696 (1996).

[12] H. Di Lorenzo Pires, F. M. G. J. Coppens, and M. P. van Exter *Type-I Spontaneous Parametric Down-Conversion with a Strongly Focused Pump* Phys. Rev. A. **83**, 033837 (2011).

[13] A. B. U'Ren, C. Silberhorn, K. Banaszek, I. A. Walmsley, R. Erdmann, W. P. Grice, and M. G. Raymer, *Generation of Pure-State Single-Photon Wavepackets by Conditional Preparation Based on Spontaneous Parametric Downconversion*, Laser Physics, **15**, pp. 146 - 161 (2005).

[14] I. H. Malitson, *Interspecimen Comparison of the Refractive Index of Fused Silica*, J. Opt. Soc. Am. **55**, pp. 1205 - 1208 (1965).

[15] S. Kasap and P. capper, eds., *Springer Handbook of Electronic and Photonic Materials* Springer, New York (2006).

[16] R.H. Stolen and e. P. Ippen, Raman Gain in Glass Optical Waveguides, Applied Physics Letters, **22**, pp. 276 - 278 (1973).

[17] K. Garay-Palmett, H.J. McGuinness, O. Cohen, J. S. Lundeen, R. Rangel-Rojo, A. B. U'Ren, M. G. Raymer, C. J. McKinstrie, S. Radic, and I. A. Walmsley, *Photon pair-state preparation with tailored spectral properties by spontaneous four-wave mixing in photonic-crystal fiber*, Opt. Express, **15**, pp. 14870 - 14886 (2007).

[18] O. Cohen, J.S. Lundeen, B. J. Smith, G. Puentes, P. J. Mosley, and I. A. Walmsley, *Tailored Photon-Pair Generation in Optical Fibers*, Phys. Rev. Lett. **102**, pp. 123603 (2009).

[19] K. Garay-Palmett, R. Rangel-Rojo, A. B. U'Ren, S. Camachol-Lopez, and R. Evans, *Generation of Photon Pairs with Tialored Spectral Properties by Spontaneous Four-Wave Mixing*, AIP Conf. Proc. **992**, 403, (2008)

[20] K. F. Lee, J. Chen, C. Liang, X. Li, P. L. Voss, and P. Kumar, *Generation of High-Purity Telcom-Band Entangled Photon Pairs in Dispersion-Shifted Fiber*, Opt. Lett., **31**, pp. 1905 - 1907 (2006).

[21] S. D. Dyer, M. J. Stevens, B. Baek, and S. W. Nam, *High-Efficiency, Ultra Low-Noise All-Fiber Photon-Pair Source*, Opt. Express, **16**, pp. 9966 - 9977 (2008).

[22] B. J. Smith, P. Mahou, O. Cohen, J.S. Lundeen, and I. A. Walmsley, *Photon pair generation in birefringent*, Opt. Express **26** pp. 23589 - 23602 (2009).

Appendix A

JOINT SPECTRAL AMPLITUDE CALCULATION

In this appendix, we show the detailed calculation for the expression of the joint spectral amplitude.

$$f(\omega_s,\omega_i) = N\int d\omega_{p1} e^{-i\omega_{p1}\tau} e^{-\left(\frac{\omega_{p1}-\omega_{p1}^0}{\sigma_{p1}}\right)^2} e^{-\left(\frac{\omega_{p2}-\omega_{p2}^0}{\sigma_{p2}}\right)^2} \int_0^L dz e^{-i\Delta k z} \tag{A.1}$$

Using

$$\int_0^L dz e^{-i\Delta k z} = \mathrm{sinc}\left(\frac{L\Delta k}{2}\right) e^{-\frac{iL\Delta k}{2}} \tag{A.2}$$

The joint spectrum can be written as:

$$f(\omega_s,\omega_i) = N\int d\omega_{p1}\ \mathrm{sinc}\left(\frac{L\Delta k}{2}\right) e^{\frac{-iL\Delta k}{2}} e^{-i\omega_{p1}\tau} e^{-\left(\frac{\omega_{p1}-\omega_p^0}{\sigma_{p1}}\right)^2} e^{-\left(\frac{\omega_{p2}-\omega_p^2}{\sigma_{p2}}\right)^2} \tag{A.3}$$

It is useful to apply the following integration transformation:

$$\omega_{p1} - \omega_{p1}^0 = \frac{\nu_s+\nu_i}{2} + \Omega \tag{A.4}$$

From this integration transformation, we can find an expression containing $\omega_{p2}-\omega_{p2}^0$ by subtracting $\nu_s+\nu_i = \omega_s - \omega_s^0 + \omega_i - \omega_i^0$ from each side

$$\Omega = \omega_{p1} - \omega_{p1}^0 - \frac{\nu_s+\nu_i}{2} - \frac{\nu_s+\nu_i}{2} + \frac{\nu_s+\nu_i}{2} \tag{A.5}$$

$$\Omega = \omega_{p1} - \omega_{p1}^0 - (\nu_s+\nu_i) + \frac{\nu_s+\nu_i}{2} \tag{A.6}$$

$$\Omega = -(\omega_{p2}-\omega_{p2}^0) + \frac{\nu_s+\nu_i}{2} \tag{A.7}$$

Momentum and energy conservation state:

$$\Delta\omega = \omega_{p1} + \omega_{p2} - \omega_s - \omega_i = 0 \tag{A.8}$$

$$\Delta k = k_{p1}(\omega_{p1}) + k_{p2}(\omega_{p2}) - k_s(\omega_s) - k_i(\omega_i) = 0 \tag{A.9}$$

Assuming that there exists values ω_{p1}^0, ω_{p2}^0, ω_s^0, and ω_i^0 such that phasematching and momentum conservation are satisfied, i.e.

$$\omega_{p1}^0 + \omega_{p2}^0 = \omega_s^0 + \omega_i^0 \tag{A.10}$$

$$k_{p1}(\omega_{p1}^0) + k_{p1}(\omega_{p2}^0) = k_s(\omega_s^0) + k_i(\omega_i^0) \tag{A.11}$$

one can use a Taylor expansion of Δk, about these values.

$$\Delta k \approx k_{p1}(\omega_{p1}^0) + k'_{p1}(\omega_{p1}^0)[\omega_{p1} - \omega_{p1}^0] + k_{p2}(\omega_{p2}^0) + k'_{p2}(\omega_{p2}^0)[\omega_{p2} - \omega_{p2}^0] \tag{A.12}$$

$$- k_s(\omega_s^0) - k'_s(\omega_s^0)[\omega_s - \omega_s^0] - k_i(\omega_i^0) - k'_i(\omega_i^0)[\omega_i - \omega_i^0] \tag{A.13}$$

where

$$k'_\mu(\omega_\mu^0) = \left.\frac{dk_\mu}{d\omega}\right|_{\omega=\omega_\mu} \tag{A.14}$$

$$\Delta k \approx k'_{p1}(\omega_{p1}^0)[\omega_{p1} - \omega_{p1}^0] + k'_{p2}(\omega_{p2}^0)[\omega_{p2} - \omega_{p2}^0] - k'_s(\omega_s^0)[\omega_s - \omega_s^0] - k'_i(\omega_i^0)[\omega_i - \omega_i^0] \tag{A.15}$$

Using the following substitutions to simplify the expression for Δk

$$\tau_p = L\left(k'_{p1}(\omega_{p1}^0) - k'_{p2}(\omega_{p2}^0)\right) \tag{A.16}$$

$$\tau_\mu = L\left(\frac{k'_{p1}(\omega_{p1}^0) + k'_{p2}(\omega_{p2}^0)}{2} - k'_\mu(\omega_\mu)\right) \text{ for } \mu = s, i \tag{A.17}$$

Δk can be written as

$$\Delta k \approx \frac{1}{L}(\nu_s\tau_s + \nu_i\tau_i + \tau_p\Omega) \tag{A.18}$$

where

$$\omega_{p1} - \omega_{p1}^0 = \frac{\nu_s + \nu_i}{2} + \Omega \tag{A.19}$$

$$\omega_{p2} - \omega_{p2}^0 = \frac{\nu_s + \nu_i}{2} - \Omega \tag{A.20}$$

$$\nu_s = \omega_s - \omega_s^0 \tag{A.21}$$

$$\nu_i = \omega_s - \omega_i^0 \tag{A.22}$$

The joint spectral amplitude in terms of ν_s and ν_i can now be written as:

$$F(\nu_s,\nu_i) = \kappa E_0^2 \int d\Omega\ e^{-i(\frac{1}{2}(\nu_s\tau_s+\nu_i\tau_i)+\frac{1}{2}\Omega\tau_p)}\mathrm{sinc}\left(\frac{1}{2}(\nu_s\tau_s+\nu_i\tau_i)+\frac{1}{2}\Omega\tau_p\right)\times$$
$$e^{-i(\omega_{p1}^0+\frac{\nu_s+\nu_i}{2}+\Omega)\tau}e^{-\left(\frac{\frac{\nu_s+\nu_i}{2}+\Omega}{\sigma_{p1}}\right)^2-\left(\frac{\frac{\nu_s+\nu_i}{2}+\Omega}{\sigma_{p2}}\right)^2}$$

$$= \kappa E_0^2\ e^{-i\frac{1}{2}\nu_s\tau}e^{-i\frac{1}{2}\nu_i\tau}e^{-i\tau\omega_{p1}^0}e^{-i\frac{1}{2}(\nu_s\tau_s+\nu_i\tau_i)}\times$$
$$\int d\Omega\ \mathrm{sinc}\left(\frac{1}{2}(\nu_s\tau_s+\nu_i\tau_i)+\frac{1}{2}\Omega\tau_p\right)e^{-i\frac{1}{2}\Omega\tau_p}e^{-i\Omega\tau}e^{-\left(\frac{\frac{\nu_s+\nu_i}{2}+\Omega}{\sigma_{p1}}\right)^2-\left(\frac{\frac{\nu_s+\nu_i}{2}-\Omega}{\sigma_{p2}}\right)^2}$$

Manipulating the power of the last exponent:

$$\begin{aligned}
&-\left(\frac{\frac{\nu_s+\nu_i}{2}+\Omega}{\sigma_{p1}}\right)^2-\left(\frac{\frac{\nu_s+\nu_i}{2}-\Omega}{\sigma_{p2}}\right)^2\\
&=-\left[\frac{(\frac{\nu_s+\nu_i}{2})^2}{\sigma_{p1}^2}+\frac{\Omega^2}{\sigma_{p1}^2}+\frac{\Omega(\nu_s+\nu_i)}{\sigma_{p1}^2}\right]-\left[\frac{(\frac{\nu_s+\nu_i}{2})^2}{\sigma_{p2}^2}+\frac{\Omega^2}{\sigma_{p2}^2}-\frac{\Omega(\nu_s+\nu_i)}{\sigma_{p2}^2}\right]\\
&=-\left(\frac{\nu_s+\nu_i}{2}+\Omega^2\right)\left(\frac{1}{\sigma_{p1}^2}+\frac{1}{\sigma_{p2}^2}\right)+\Omega(\nu_s+\nu_i)\left(\frac{1}{\sigma_{p2}^2}-\frac{1}{\sigma_{p1}^2}\right)\\
&=-\frac{1}{\sigma^2}\left(\frac{\nu_s+\nu_i}{2}\right)^2-\frac{\Omega^2}{\sigma^2}+\frac{\Omega(\nu_s+\nu_i)}{\Sigma^2}
\end{aligned}\tag{A.23}$$

where

$$\frac{1}{\sigma^2}=\frac{1}{\sigma_{p1}}+\frac{1}{\sigma_{p2}}\tag{A.24}$$

$$\frac{1}{\Sigma^2}=\frac{1}{\sigma_{p1}}-\frac{1}{\sigma_{p2}}\tag{A.25}$$

The joint spectral amplitude is thus,

$$\begin{aligned}
F(\nu_s,\nu_i) =&\kappa E_0^2\ e^{-i\frac{1}{2}\nu_s\tau}e^{-i\frac{1}{2}\nu_i\tau}e^{-i\tau\omega_{p1}^0}e^{-i\frac{1}{2}(\nu_s\tau_s+\nu_i\tau_i)}e^{-\frac{1}{\sigma^2}(\frac{\nu_s+\nu_i}{2})^2}\times\\
&\int d\Omega\ \mathrm{sinc}\left(\frac{1}{2}(\nu_s\tau_s+\nu_i\tau_i)+\frac{1}{2}\Omega\tau_p\right)e^{-i\Omega(\frac{1}{2}\tau_p+\tau)}e^{-\frac{\Omega^2}{\sigma^2}+\frac{\Omega(\nu_s+\nu_i)}{\Sigma^2}}
\end{aligned}$$

Manipulating the power of the last exponent:

$$
\begin{aligned}
&-\frac{\Omega^2}{\sigma^2} + (\frac{\nu_s+\nu_i}{\Sigma^2})\Omega \\
&= -\frac{1}{\sigma^2}\left(\Omega^2 - \frac{\sigma^2}{\Sigma^2}\left(\nu_s+\nu_i\right)\Omega + \left[\frac{\sigma^2}{\Sigma^2}\frac{\nu_s+\nu_i}{2}\right]^2\right) + \left[\frac{\sigma^2}{\Sigma^2}\frac{\nu_s+\nu_i}{2}\right]^2 \\
&= -\frac{1}{\sigma^2}\left(\Omega - \frac{\sigma^2}{\Sigma^2}\left(\frac{\nu_s+\nu_i}{2}\right)\right)^2 + \frac{\sigma^2}{\Sigma^2}\left(\frac{\nu_s+\nu_i}{2}\right)^2
\end{aligned}
$$

$$
\begin{aligned}
F(\nu_s,\nu_i) =& \kappa E_0^2\ e^{-i\frac{1}{2}\nu_s\tau}e^{-i\frac{1}{2}\nu_i\tau}e^{-i\tau\omega_{p1}^0}e^{-i\frac{1}{2}(\nu_s\tau_s+\nu_i\tau_i)}e^{-(\frac{1}{\sigma^2}-\frac{\sigma^2}{\Sigma^2})(\frac{\nu_s+\nu_i}{2})^2}\times \\
&\int d\Omega\ \mathrm{sinc}\left(\frac{1}{2}(\nu_s\tau_s+\nu_i\tau_i)+\frac{1}{2}\Omega\tau_p\right)e^{-i\Omega(\frac{1}{2}\tau_p+\tau)}e^{-\frac{1}{\sigma^2}(\Omega-\frac{\sigma^2}{\Sigma^2}(\frac{\nu_s+\nu_i}{2}))^2}
\end{aligned}
$$

Using $t = \frac{1}{2}\tau_p + \tau$, $\frac{1}{\sigma^2} - \frac{\sigma^2}{\Sigma^4} = \frac{4}{\sigma_1^2+\sigma_2^2}$, and $\alpha = \frac{1}{2}(\nu_s\tau_s + \nu_i\tau_i)$, we arrive at

$$
\begin{aligned}
F(\nu_s,\nu_i) = \kappa E_0^2\ & e^{-i\frac{1}{2}\nu_s\tau}e^{-i\frac{1}{2}\nu_i\tau}e^{-i\tau\omega_{p1}^0}e^{-i\frac{1}{2}(\nu_s\tau_s+\nu_i\tau_i)}e^{-\frac{(\nu_s+\nu_i)^2}{\sigma_1^2+\sigma_2^2}}\times \\
&\int d\Omega\ e^{-i\Omega t}\ \mathrm{sinc}(\alpha+\Omega(t-\tau))\ \ e^{-\frac{1}{\sigma^2}(\Omega-\frac{\sigma^2}{\Sigma^2}(\frac{\nu_s+\nu_i}{2}))^2}
\end{aligned}
\tag{A.26}
$$

Using the Convolution theorem, where F is the Fourier Transform:

$$
\begin{aligned}
F\{f*g\} &= F(f)\cdot F(g) \\
(f*g)(t) &= \int_{-\infty}^{\infty} f(t')g(t-t')dt'
\end{aligned}
$$

$$
F(f) = f(t) = \int d\Omega\ e^{-i\Omega t}e^{\frac{1}{\sigma^2}(\Omega-\frac{\sigma^2}{\Sigma^2}(\frac{\nu_s+\nu_i}{2}))^2}
$$

Let $u = \Omega - \frac{\sigma^2}{\Sigma^2}(\frac{\nu_s+\nu_i}{2})$,

$$
\int du\ e^{-it(\frac{\sigma^2}{\Sigma^2}(\frac{\nu_s+\nu_i}{2}))}e^{-itu}e^{-\frac{u^2}{\sigma^2}}
$$

using $\int dx e^{-\alpha x^2}e^{-i\omega x} = \sqrt{\frac{\pi}{\alpha}}e^{-\frac{\omega^2}{4\alpha}}$, where $\alpha = \frac{1}{\sigma^2}$

$$
f(t) = \sigma\sqrt{\pi}\ e^{-\frac{t^2\sigma^2}{4}}e^{-it(\frac{\sigma^2}{\Sigma^2}(\frac{\nu_s+\nu_i}{2}))} \tag{A.27}
$$

Whereas $F(g)$ is:

$$
F(g) = g(t) = \int d\Omega\ e^{-i\Omega t}\ \mathrm{sinc}(\alpha+\Omega(t-\tau))
$$

Let $w = \frac{\alpha}{t-\tau} + \Omega$

$$\int dw\ e^{-it(w-\frac{\alpha}{t-\tau})}\ \mathrm{sinc}[(t-\tau)w]$$
$$= e^{\frac{it\alpha}{t-\tau}} \int dw\ e^{-itw}\ \mathrm{sinc}[(t-\tau)w]$$

using $\int dw\ e^{-itw}\ \mathrm{sinc}(\frac{wa}{2}) = \frac{2\pi}{a}\ \mathrm{rect}(\frac{t}{a})$, where $a = 2(t-\tau) = \tau_p$

$$g(t) = e^{\frac{it\alpha}{t-\tau}} \frac{\pi}{(t-\tau)}\ \mathrm{rect}\left(\frac{t}{2(t-\tau)}\right) \tag{A.28}$$

$$g(t) = e^{\frac{it(\nu_s\tau_s+\nu_i\tau_i)}{\tau_p}} \frac{2\pi}{\tau_p}\ \mathrm{rect}\left(\frac{t}{\tau_p}\right) \tag{A.29}$$

Therefore,

$$\{f * g\} = \int_{-\infty}^{\infty} dt'\ e^{i(t-t')(\frac{\nu_s\tau_s+\nu_i\tau_i}{\tau_p})} \frac{2\pi}{\tau_p}\ \mathrm{rect}\left(\frac{t-t'}{\tau_p}\right) \times$$
$$\sigma\sqrt{\pi} e^{-\frac{t'^2\sigma^2}{4}} e^{-it'(\frac{\sigma^2}{\Sigma^2}(\frac{\nu_s+\nu_i}{2}))}$$

where, because of the rect function:

$$-\frac{1}{2} < \frac{t-t'}{|\tau_p|} < \frac{1}{2}$$

Thus,

$$\{f * g\} = e^{it\frac{\nu_s\tau_s+\nu_i\tau_i}{\tau_p}} \frac{\sigma}{\tau_p} 2\pi^{\frac{3}{2}} \int_{-\frac{1}{2}|\tau_p|+t}^{\frac{1}{2}|\tau_p|+t} dt'\ e^{-\left(\frac{t'^2\sigma^2}{4}\right)} e^{-it'\left(\frac{\nu_s\tau_s+\nu_i\tau_i}{\tau_p} + \frac{\sigma^2}{\Sigma^2}(\frac{\nu_s+\nu_i}{2})\right)}$$
$$= e^{it\frac{\nu_s\tau_s+\nu_i\tau_i}{\tau_p}} \frac{\sigma}{\tau_p} 2\pi^{\frac{3}{2}} \int_{-\frac{1}{2}|\tau_p|+t}^{\frac{1}{2}|\tau_p|+t} dt'\ e^{-\left(\frac{t'^2\sigma^2}{4} + it'\left(\frac{\nu_s\tau_s+\nu_i\tau_i}{\tau_p} + \frac{\sigma^2}{\Sigma^2}(\frac{\nu_s+\nu_i}{2})\right)\right)}$$

$$\{f*g\} = \; e^{it\frac{\nu_s\tau_s+\nu_i\tau_i}{\tau_p}}\frac{\sigma}{\tau_p}2\pi^{\frac{3}{2}}\int_{-\frac{1}{2}|\tau_p|+t}^{\frac{1}{2}|\tau_p|+t}dt'\; e^{-\frac{\sigma^2}{4}\left(t'^2+\frac{i4t'}{\sigma^2}\left(\frac{\nu_s\tau_s+\nu_i\tau_i}{\tau_p}+\frac{\sigma^2}{\Sigma^2}(\frac{\nu_s+\nu_i}{2})\right)\right)}$$

$$= \; e^{it\frac{\nu_s\tau_s+\nu_i\tau_i}{\tau_p}}\frac{\sigma}{\tau_p}2\pi^{\frac{3}{2}}\times$$
$$\int_{-\frac{1}{2}|\tau_p|+t}^{\frac{1}{2}|\tau_p|+t}dt'\; e^{-\frac{\sigma^2}{4}\left(t'^2+\frac{i4t'}{\sigma^2}\left(\frac{\nu_s\tau_s+\nu_i\tau_i}{\tau_p}+\frac{\sigma^2}{\Sigma^2}(\frac{\nu_s+\nu_i}{2})\right)-\frac{4}{\sigma^4}\left(\frac{\nu_s\tau_s+\nu_i\tau_i}{\tau_p}+\frac{\sigma^2}{\Sigma^2}(\frac{\nu_s+\nu_i}{2})\right)^2\right)}\times$$
$$e^{-\frac{1}{\sigma^2}\left(\frac{\nu_s\tau_s+\nu_i\tau_i}{\tau_p}+\frac{\sigma^2}{\Sigma^2}(\frac{\nu_s+\nu_i}{2})\right)^2}$$

$$= e^{it\frac{\nu_s\tau_s+\nu_i\tau_i}{\tau_p}}\frac{\sigma}{\tau_p}2\pi^{\frac{3}{2}}\times$$
$$\int_{-\frac{1}{2}|\tau_p|+t}^{\frac{1}{2}|\tau_p|+t}dt'\; e^{-\frac{\sigma^2}{4}\left(t'-\frac{2t'i}{\sigma^2}\left(\frac{\nu_s\tau_s+\nu_i\tau_i}{\tau_p}+\frac{\sigma^2}{\Sigma^2}(\frac{\nu_s+\nu_i}{2})\right)\right)^2}e^{-\frac{1}{\sigma^2}\left(\frac{\nu_s\tau_s+\nu_i\tau_i}{\tau_p}+\frac{\sigma^2}{\Sigma^2}(\frac{\nu_s+\nu_i}{2})\right)^2}$$

$$= e^{it\frac{\nu_s\tau_s+\nu_i\tau_i}{\tau_p}}e^{-\frac{1}{\sigma^2}\left(\frac{\nu_s\tau_s+\nu_i\tau_i}{\tau_p}+\frac{\sigma^2}{\Sigma^2}(\frac{\nu_s+\nu_i}{2})\right)^2}\frac{\sigma}{\tau_p}2\pi^{\frac{3}{2}}\times$$
$$\int_{-\frac{1}{2}|\tau_p|+t}^{\frac{1}{2}|\tau_p|+t}dt'\; e^{-\frac{\sigma^2}{4}\left(t'-\frac{2i}{\sigma^2}\left(\frac{\nu_s\tau_s+\nu_i\tau_i}{\tau_p}+\frac{\sigma^2}{\Sigma^2}(\frac{\nu_s+\nu_i}{2})\right)\right)^2}$$

let $u = t' + \frac{2i}{\sigma^2}\left(\frac{\nu_s\tau_s+\nu_i\tau_i}{\tau_p} + \frac{\sigma^2}{\Sigma^2}(\frac{\nu_s+\nu_i}{2})\right)$

$$\{f*g\} = e^{it\frac{\nu_s\tau_s+\nu_i\tau_i}{\tau_p}}e^{-\frac{1}{\sigma^2}(\frac{\nu_s\tau_s+\nu_i\tau_i}{\tau_p}+\frac{\sigma^2}{\Sigma^2}(\frac{\nu_s+\nu_i}{2}))^2}\frac{\sigma}{\tau_p}2\pi^{\frac{3}{2}}\times$$
$$\int_{-\frac{1}{2}|\tau_p|+\frac{1}{2}\tau_p+\tau+\frac{2i}{\sigma^2}(\frac{\nu_s\tau_s+\nu_i\tau_i}{\tau_p}+\frac{\sigma^2}{\Sigma^2}(\frac{\nu_s+\nu_i}{2}))}^{\frac{1}{2}|\tau_p|+\frac{1}{2}\tau_p+\tau+\frac{2i}{\sigma^2}(\frac{\nu_s\tau_s+\nu_i\tau_i}{\tau_p}+\frac{\sigma^2}{\Sigma^2}(\frac{\nu_s+\nu_i}{2}))}du\; e^{-\frac{\sigma^2}{4}u^2}$$

letting $w = \frac{\sigma}{2}u$, carrying out the integration, and recalling that $t = \frac{1}{2}\tau_p + \tau$,

$$\{f * g\} = e^{it\frac{\nu_s\tau_s+\nu_i\tau_i}{\tau_p}} e^{-\frac{1}{\sigma^2}\left(\frac{\nu_s\tau_s+\nu_i\tau_i}{\tau_p}+\frac{\sigma^2}{\Sigma^2}(\frac{\nu_s+\nu_i}{2})\right)^2} \frac{\sigma}{\tau_p} 2\pi^{\frac{3}{2}} \times$$
$$\frac{2}{\sigma}\left(\mathrm{erf}\left[\frac{\sigma(\tau_p+\tau)}{2} + \frac{2i}{\sigma^2}\left(\frac{\nu_s\tau_s+\nu_i\tau_i}{\tau_p} + \frac{\sigma^2}{\Sigma^2}\frac{\nu_s+\nu_i}{2}\right)\right] - \right.$$
$$\left. \mathrm{erf}\left[\frac{\sigma\tau}{2} + \frac{2i}{\sigma^2}\left(\frac{\nu_s\tau_s+\nu_i\tau_i}{\tau_p} + \frac{\sigma^2}{\Sigma^2}\frac{\nu_s+\nu_i}{2}\right)\right]\right)$$

$$\{f * g\} = \pi^{\frac{3}{2}}\frac{1}{\tau_p} e^{i(\frac{1}{2}\tau_p+\tau)\frac{\nu_s\tau_s+\nu_i\tau_i}{\tau_p}} e^{-\frac{1}{\sigma^2}(\frac{\nu_s\tau_s+\nu_i\tau_i}{\tau_p})^2 - \frac{\sigma}{\Sigma^4}(\frac{\nu_s+\nu_i}{2})^2 - \frac{\sigma}{\Sigma^2}(\nu_s+\nu_i)} \times$$
$$\mathrm{erf}\left(\frac{\sigma(\tau_p+\tau)}{2} + i\frac{T_s\nu_s + T_i\nu_i}{\sigma\tau_p}\right) - \mathrm{erf}\left(\frac{\sigma\tau}{2} + i\frac{T_s\nu_s + T_i\nu_i}{\sigma\tau_p}\right)$$

where

$$T_\mu = \tau_\mu + \frac{\sigma^2}{2\Sigma^2}\tau_p = \tau_\mu + \frac{1}{2}\frac{\sigma_1^2 - \sigma_2^2}{\sigma_1^2 + \sigma_2^2}\tau_p$$

The joint spectral amplitude is thus:

$$F(\nu_s,\nu_i) = N\pi^{\frac{3}{2}}\frac{1}{\tau_p} e^{-i\frac{1}{2}\nu_s\tau} e^{-i\frac{1}{2}\nu_i\tau} e^{-i\tau\omega_{p1}^0} e^{-i\frac{1}{2}(\nu_s\tau_s+\nu_i\tau_i)} e^{-\frac{(\nu_s+\nu_i)^2}{\sigma_1^2+\sigma_2^2}} \times$$
$$e^{i(\frac{1}{2}\tau_p+\tau)\frac{\nu_s\tau_s+\nu_i\tau_i}{\tau_p}} e^{-\frac{1}{\sigma^2}(\frac{\nu_s\tau_s+\nu_i\tau_i}{\tau_p})^2 - \frac{\sigma}{\Sigma^4}(\frac{\nu_s+\nu_i}{2})^2 - \frac{\sigma}{\Sigma^2}(\nu_s+\nu_i)} \times$$
$$\mathrm{erf}\left(\frac{\sigma(\tau_p+\tau)}{2} + i\frac{T_s\nu_s + T_i\nu_i}{\sigma\tau_p}\right) - \mathrm{erf}\left(\frac{\sigma\tau}{2} + i\frac{T_s\nu_s + T_i\nu_i}{\sigma\tau_p}\right)$$

$$F(\nu_s,\nu_i) = N\pi^{\frac{3}{2}}\frac{1}{\tau_p} e^{-i(\frac{1}{2}(\nu_s\tau_s+\nu_i\tau_i)+\omega_{p1}^0\tau+(\frac{\nu_s+\nu_i}{2})\tau)} e^{-\left[\frac{1}{\sigma^2}+\frac{\sigma^2}{\Sigma^4}\right]\left(\frac{\nu_s+\nu_i}{2}\right)^2}$$
$$e^{it\frac{\nu_s\tau_s+\nu_i\tau_i}{\tau_p}} e^{-\frac{1}{\sigma^2}\left(\frac{\nu_s\tau_s+\nu_i\tau_i}{\tau_p}\right)^2 + \left(\frac{\sigma^2}{\Sigma^2}\left(\frac{\nu_s+\nu_i}{2}\right)\right)^2 + \frac{\sigma^2}{\Sigma^2}(\nu_s+\nu_i)}$$
$$\times \mathrm{erf}\left(\frac{\sigma(\tau_p+\tau)}{2} + i\frac{T_s\nu_s + T_i\nu_i}{\sigma\tau_p}\right) - \mathrm{erf}\left(\frac{\sigma\tau}{2} + i\frac{T_s\nu_s + T_i\nu_i}{\sigma\tau_p}\right)$$

A.1 Regime 1 calculation

$$f(\omega_s,\omega_i) = N\int_0^L dz e^{-i\Delta kz}\int d\omega_{p1} e^{-i\omega_{p1}\tau} e^{-\left(\frac{\omega_{p1}-\omega_{p1}^0}{\sigma_{p1}}\right)^2} e^{-\left(\frac{\omega_s+\omega_i-\omega_{p1}-\omega_{p2}^0}{\sigma_{p2}}\right)^2} \quad \text{(A.30)}$$

where

$$\int_0^L dz\ \exp\Bigg[-\left(\frac{\sigma\tau_p z}{2L}+\left(\frac{\sigma\tau}{2}+i\frac{T_s\nu_s+T_i\nu_i}{\sigma\tau_p}\right)\right)^2\Bigg] \tag{A.31}$$

$$=\frac{2L}{\sigma\tau_p}\int_{\frac{\sigma\tau}{2}}^{\frac{\sigma(\tau_p+\tau)}{2}} dt\ \exp\Bigg[-\left(t+i\frac{T_s\nu_s+T_i\nu_i}{\sigma\tau_p}\right)\Bigg] \tag{A.32}$$

$$=\frac{2L}{\sigma\tau_p}e^{\left(\frac{T_s\nu_s+T_i\nu_i}{\sigma\tau_p}\right)^2}\int_{\frac{\sigma\tau}{2}}^{\frac{\sigma(\tau_p\tau)}{2}} dt\ \exp\Bigg[-t^2-2it\frac{T_s\nu_s+T_i\nu_i}{\sigma\tau_p}\Bigg] \tag{A.33}$$

$$\approx\frac{2L}{\sigma\tau_p}e^{\left(\frac{T_s\nu_s+T_i\nu_i}{\sigma\tau_p}\right)^2}\frac{\sigma\tau_p}{2}e^{-i(\frac{\tau}{\tau_p}+\frac{1}{2})(T_s\nu_s+T_i\nu_i)}\ \mathrm{sinc}\left(\frac{T_s\nu_s+T_i\nu_i}{2}\right) \tag{A.34}$$

$$\approx Le^{\left(\frac{T_s\nu_s+T_i\nu_i}{\sigma\tau_p}\right)^2}e^{-i(\frac{\tau}{\tau_p}+\frac{1}{2})(T_s\nu_s+T_i\nu_i)}\ \mathrm{sinc}\left(\frac{T_s\nu_s+T_i\nu_i}{2}\right) \tag{A.35}$$

The length of the fiber can be absorbed in the normalization constant. Therefore, negligible temporal walk-off between the two pumps ($|\sigma\tau_p| << 1$) coupled with ensuring the pump beams interact in the fiber $|(\sigma\tau| << 1$) simplify the joint spectral amplitude to

$$F(\nu_s,\nu_i)=N\pi^{\frac{3}{2}}e^{-i\omega_{p1}^0\tau}e^{-i\tau(\nu_s+\nu_i)\frac{\sigma_1^2-\sigma_2^2}{\sigma_1^2+\sigma_2^2}}e^{-i\frac{T_s\nu_s+T_i\nu_i}{2}}\ \mathrm{sinc}\left(\frac{T_s\nu_s+T_i\nu_i}{2}\right) \tag{A.36}$$

A.2 Regime 2 calculation

$$f(\omega_s,\omega_i)=N\int_0^L dz e^{-i\Delta kz}\int d\omega_{p1}e^{-i\omega_{p1}\tau}e^{-\left(\frac{\omega_{p1}-\omega_{p1}^0}{\sigma_{p1}}\right)^2}e^{-\left(\frac{\omega_s+\omega_i-\omega_{p1}-\omega_{p2}^0}{\sigma_{p2}}\right)^2} \tag{A.37}$$

where

$$\int_0^L dz\ \exp\Bigg[-\left(\frac{\sigma\tau_p z}{2L}+\left(\frac{\sigma\tau}{2}+i\frac{T_s\nu_s+T_i\nu_i}{\sigma\tau_p}\right)\right)^2\Bigg] \tag{A.38}$$

$$=\frac{2L}{\sigma\tau_p}\int_{\frac{\sigma\tau}{2}}^{\frac{\sigma(\tau+\tau_p)}{2}} dt\ \exp\Bigg[-\left(t+i\frac{T_s\nu_s+T_i\nu_i}{\sigma\tau_p}\right)^2\Bigg] \tag{A.39}$$

$$\approx\frac{2L}{|\sigma\tau_p|}\int_{-\infty}^{\infty} dt\ \exp\Bigg[-\left(t+i\frac{T_s\nu_s+T_i\nu_i}{\sigma\tau_p}\right)^2\Bigg] \tag{A.40}$$

$$=\frac{2L\sqrt{\pi}}{|\sigma\tau_p|} \tag{A.41}$$

Therefore, the joint spectral amplitude in this regime is

$$F(\nu_s,\nu_i) = \left[N\pi^{\frac{5}{2}}\frac{\sigma_1\sigma_2}{|\sigma\tau_p|}\frac{1}{\sqrt{\sigma_1^2+\sigma_2^2}}e^{-i\omega_{p1}^0\tau}e^{-i\frac{1}{2}\nu_s\tau}e^{-i\frac{1}{2}\nu_i\tau}e^{i\frac{\tau}{\tau_p}(\nu_s\tau_s+\nu_i\tau_i)}\right]\times$$
$$e^{-\frac{(\nu_s+\nu_i)^2}{\sigma_1^2+\sigma_2^2}}e^{-\left(\frac{T_s\nu_s+T_i\nu_i}{\sigma\tau_p}\right)^2} \tag{A.42}$$